

**FINAL YEAR PROJECT**

**DEPARTMENT OF COMPUTING**

**IMPERIAL COLLEGE OF SCIENCE, TECHNOLOGY AND MEDICINE**

---

**Estimating Regional AADT and GHG  
Emissions from Satellite Imagery**

---

*Author:*  
Adam Horsler

*Supervisor:*  
Dr. Pedro Baiz  
*Second marker:*  
Prof William Knottenbelt

June 21, 2023

Submitted in partial fulfillment of the requirements for the MEng of Imperial  
College London

## Abstract

This project presents a novel two-part pipeline for monitoring progress towards the UN Sustainable Development Goals (SDG's) related to Climate Action and Sustainable Cities and Communities. The pipeline consists of two main parts: the first part takes a raw satellite image of a motorway section and produces traffic count predictions for count sites within the image; the second part takes these predicted traffic counts and produces estimates of Local Authority (LA) level motorway Average Annual Daily Traffic (AADT) on a per vehicle type basis and Greenhouse Gas (GHG) emissions. We also extend the pipeline to introduce a novel method for estimating emissions when data on AADT per vehicle type is not available, include LA A-Roads and minor roads AADT and GHG emissions, and perform parametric analysis on parameters used in the pipeline. We treat the 2017 year as training and 2018 as the test year. Results show that it is possible to predict AADT and GHG emissions from satellite imagery, with motorway test year  $R^2$  values of 0.92 and 0.78 respectively, and for A-roads'  $R^2$  values of 0.94 and 0.98. This end-to-end two-part pipeline builds upon previous research in road transportation traffic flows, speed estimation from satellite imagery, and emissions estimation, providing new contributions and insights into these areas.

---

## Acknowledgments

I would like to acknowledge my supervisor, Dr. Pedro Baiz, who has provided invaluable assistance and support throughout the project.

I would also like to thank Dr. Thomas Lancaster for the overall support to projects in the Department of Computing.

Finally, I would like to greatly thank my friends and family for their support and encouragement throughout the project.

# Contents

<b>1</b>	<b>Introduction</b>	<b>2</b>
1.1	Motivation . . . . .	2
1.2	Objectives . . . . .	2
1.3	Contributions . . . . .	3
<b>2</b>	<b>Background</b>	<b>4</b>
2.1	Datasets . . . . .	4
2.1.1	Road Transport and Traffic Data . . . . .	4
2.1.2	Satellite Imagery Data for Road Transport . . . . .	5
2.1.3	Greenhouse Gas Emissions Data for Road Transport . . . . .	5
2.2	Deep Learning Models . . . . .	6
2.2.1	Artificial Neural Networks (ANN) . . . . .	6
2.2.2	Convolutional Neural Networks (CNN's) for Object Detection . . . . .	7
2.2.3	Evaluation Metrics . . . . .	8
2.3	Modelling Methodologies . . . . .	9
2.3.1	Satellite Imagery Pre-Processing . . . . .	9
2.3.2	Vehicle Detection from Satellite Imagery . . . . .	10
2.3.3	Traffic Counts . . . . .	10
2.3.4	Annual Average Daily Traffic (AADT) Flow . . . . .	11
2.3.5	Road Transport Greenhouse Gas Emissions . . . . .	11
2.3.6	Evaluation Metrics . . . . .	12
2.4	Pipeline Overview . . . . .	12
2.4.1	Datasets Summary . . . . .	13
2.4.2	DL Models Summary . . . . .	14
2.4.3	Modelling Summary . . . . .	14
<b>3</b>	<b>Exploratory Data Analysis</b>	<b>16</b>
3.1	Motorway Road Transport . . . . .	16
3.1.1	15-Minute Traffic Counts . . . . .	16
3.1.2	Local Authority AADT . . . . .	17
3.2	Satellite Imagery for Road Transport . . . . .	19
3.2.1	Specifications . . . . .	19
3.2.2	xView for Model Training . . . . .	19
3.2.3	European Space Imaging . . . . .	20
3.3	Motorway GHG Emissions . . . . .	21
3.3.1	Local Authority GHG Emissions . . . . .	21

3.4	Motorways Summary . . . . .	22
3.5	Extension to Other Road Types . . . . .	23
<b>4</b>	<b>Implementation of Motorway Traffic Counts</b>	<b>26</b>
4.1	Chosen Count Sites . . . . .	27
4.2	WV-2 Satellite Image Pre-Processing . . . . .	27
4.3	Road Vehicle Object Detection . . . . .	29
4.3.1	Model Training and Validation . . . . .	29
4.3.2	Model Inference . . . . .	30
4.4	Live Speed Estimation . . . . .	31
4.4.1	PCA-Based Method . . . . .	32
4.4.2	Results . . . . .	33
4.5	15-Minute Traffic Counts . . . . .	34
4.5.1	Results . . . . .	34
4.6	Evaluation . . . . .	35
<b>5</b>	<b>Implementation of LA AADT and GHG Emissions</b>	<b>37</b>
5.1	Motorway LA AADT . . . . .	37
5.1.1	ANN Traffic Data Pre-Processing . . . . .	37
5.1.2	ANN Training and Validation . . . . .	38
5.1.3	AADT Prediction . . . . .	39
5.1.4	Results . . . . .	39
5.2	Motorway LA GHG Emissions . . . . .	41
5.2.1	Emissions Calculation . . . . .	41
5.2.2	Results . . . . .	42
5.3	Motorway Evaluation . . . . .	43
5.3.1	Implementation without Vehicle Type Data . . . . .	44
5.4	Parametric Analysis . . . . .	46
5.4.1	LA AADT Statistics . . . . .	46
5.4.2	Traffic Counts and Speed . . . . .	47
5.4.3	GHG Emissions Variables . . . . .	49
5.5	Extension to Other Road Types . . . . .	49
5.5.1	A-Roads Results . . . . .	50
5.5.2	Evaluation . . . . .	51
<b>6</b>	<b>Ethical issues</b>	<b>53</b>
<b>7</b>	<b>Conclusions and Future Work</b>	<b>54</b>
7.1	Conclusion . . . . .	54
7.1.1	Motorway Traffic Counts . . . . .	54
7.1.2	LA AADT . . . . .	56
7.1.3	LA GHG Emissions . . . . .	56
7.2	Future Work . . . . .	57
<b>A</b>	<b>Satellite Imagery Datasets Summary</b>	<b>63</b>
<b>B</b>	<b>Chosen LA's Maximum Count Site AADT Values 2017 and 2018 Years</b>	<b>64</b>

---

---

<b>C Chosen LA's AADT Vehicle Type Distributions</b>	<b>67</b>
<b>D A-Roads LA AADT and GHG Emissions Per Year</b>	<b>69</b>
<b>E Minor Roads LA AADT and GHG Emissions Per Year</b>	<b>70</b>
<b>F Havering A-Roads and Minor Roads Vehicle Distributions</b>	<b>71</b>
<b>G Chosen LA WV-2 Satellite Images Before Processing</b>	<b>72</b>
<b>H Chosen LA WV-2 Satellite Images After Processing</b>	<b>75</b>
<b>I YOLOv5 Road Vehicle xView Training Results</b>	<b>77</b>
<b>J ANN AADT Model Architecture</b>	<b>78</b>
<b>K LA AADT Training and Validation Curves</b>	<b>79</b>
<b>L Motorways No Vehicle Type Scatter Plot</b>	<b>82</b>
<b>M Traffic Counts and Speed AADT Parametric Analysis</b>	<b>83</b>
<b>N A-Roads ANN AADT Training and Validation Curves</b>	<b>85</b>
<b>O A-Roads LA AADT and GHG Emissions Results</b>	<b>89</b>
<b>P Minor Roads LA AADT and GHG Emissions Results</b>	<b>91</b>

# List of Figures

2.1 ANN with one hidden layer [21] . . . . .	6
2.2 Intersection Over Union Illustration [25] . . . . .	8
2.3 Full Pipeline Diagram . . . . .	13
3.1 LA Maximum AADT's per year . . . . .	18
3.2 LA AADT Count Site Havering Histograms . . . . .	18
3.3 Havering LA AADT by Vehicle Type . . . . .	19
3.4 xView Training Set Example . . . . .	20
3.5 EU Space Imaging GUI . . . . .	20
3.6 LA GHG Emissions per year . . . . .	22
3.7 Motorway LA AADT and GHG Emissions Scatter Plot . . . . .	23
3.8 LA A-Roads AADT vs GHG Emissions Scatter Plot . . . . .	24
3.9 LA Minor Roads AADT vs GHG Emissions Scatter Plot . . . . .	24
4.1 Havering MS1 WV-2 Satellite Image . . . . .	28
4.2 Havering M25/5790A and M25/5790B WV-2 Processed Images . . . . .	29
4.3 xView road vehicles example training batch . . . . .	30
4.4 Havering Object Detection Zoomed Section . . . . .	31
4.5 Zoomed Section of Havering PC Change Image (left) and Vehicle Centroids Detection (Right) . . . . .	33
4.6 Live Speed Estimation MAPE Bar Chart . . . . .	33
4.7 15 Minute Traffic Count True vs Predicted Values Scatter Plot . . . . .	35
4.8 Speed Data 15-Minute Traffic Count MAPE Comparison . . . . .	36
5.1 Havering M25/5790A LA AADT Training and Validation Curves . . . . .	39
5.2 LA Predicted vs True AADT Scatter plot (top) and AADT MAPE by Vehicle type (bottom) . . . . .	41
5.3 LA Mean Predicted vs True GHG Scatter Plot . . . . .	43
5.4 LA AADT and GHG Scatter Plot . . . . .	44
5.5 MAPE Comparison for emissions calculations without Vehicle Type Data	45
5.6 MAPE Comparison of Different Statistics for LA AADT . . . . .	47
5.7 Effect of Traffic Counts and Speed on GHG Emissions MAPE . . . . .	48
5.8 LA Motorway GHG Emissions MAPE by Fuel Consumption Parameter	49
5.9 LA A-Roads AADT vs GHG Emissions Scatter Plot . . . . .	51
5.10 LA AADT and GHG MAPE By Road Type Comparison . . . . .	52
B.1 Trafford AADT Count Site Histograms . . . . .	64

B.2 Luton AADT Count Site Histograms . . . . .	65
B.3 Hounslow AADT Count Site Histograms . . . . .	66
B.4 Blackburn AADT Count Site Histograms . . . . .	66
C.1 Chosen LA's AADT by Vehicle Type Distributions . . . . .	68
D.1 LA A-Roads AADT and GHG per year . . . . .	69
E.1 LA Minor Roads AADT and GHG Emissions per year . . . . .	70
F.1 Havering A-Roads and Minor Roads Vehicle Type Distributions . . . . .	71
G.1 Trafford LA WV-2 Satellite Image Before Processing . . . . .	72
G.2 Luton LA WV-2 Satellite Image Before Processing . . . . .	73
G.3 Hounslow LA WV-2 Satellite Image Before Processing . . . . .	73
G.4 Blackburn LA WV-2 Satellite Image Before Processing . . . . .	74
H.1 Trafford LA WV-2 Satellite Images After Processing . . . . .	75
H.2 Luton LA WV-2 Satellite Images After Processing . . . . .	75
H.3 Hounslow LA WV-2 Satellite Images After Processing . . . . .	76
H.4 Blackburn LA WV-2 Satellite Images After Processing . . . . .	76
I.1 YOLOv5 Training Results . . . . .	77
J.1 ANN AADT Model Architecture . . . . .	78
K.1 Trafford M60/9083A LA Train and Val Curves . . . . .	79
K.2 Trafford M60/9083B LA Train and Val Curves . . . . .	79
K.3 Luton M1/2557A LA Train and Val Curves . . . . .	79
K.4 Luton M1/2557B LA Train and Val Curves . . . . .	80
K.5 Hounslow M4/2188A LA Train and Val Curves . . . . .	80
K.6 Hounslow M4/2188B LA Train and Val Curves . . . . .	80
K.7 Blackburn 30361032 LA Train and Val Curves . . . . .	80
K.8 Blackburn 30361033 LA Train and Val Curves . . . . .	81
L.1 Motorways No Vehicle Type Scatter Plot . . . . .	82
M.1 Effect of Traffic Counts on AADT MAPE . . . . .	83
M.2 Effect of Speed on AADT MAPE . . . . .	84
N.1 Havering M25/590A LA A-Roads Train and Val Curves . . . . .	85
N.2 Havering M25/590A LA A-Roads Train and Val Curves . . . . .	85
N.3 Trafford M60/9083A LA A-Roads Train and Val Curves . . . . .	85
N.4 Trafford M60/9083B LA A-Roads Train and Val Curves . . . . .	86
N.5 Luton M1/2557A LA A-Roads Train and Val Curves . . . . .	86
N.6 Luton M1/2557B LA A-Roads Train and Val Curves . . . . .	86
N.7 Hounslow M4/2188A LA A-Roads Train and Val Curves . . . . .	86
N.8 Hounslow M4/2188B LA A-Roads Train and Val Curves . . . . .	87
N.9 Blackburn 30361032 LA A-Roads Train and Val Curves . . . . .	87

N.10 Blackburn 30361033 LA A-Roads Train and Val Curves . . . . .	87
N.11 Luton M1/2557A LA A-Roads AADT Training and Validation Curves .	87
N.12 Luton M1/2557B LA A-Roads AADT Training and Validation Curves .	88
O.1 LA A-Roads Predicted vs True AADT (top) and GHG Emissions (bottom) Scatter Plots . . . . .	90
P.1 Minor Roads AADT Scatter Plot Results . . . . .	91
P.2 Minor Roads GHG Emissions Scatter Plot Results . . . . .	92
P.3 Minor Roads AADT vs GHG Results . . . . .	92

# Acronyms

**Table 1:** Acronyms

Acronym/Abbreviation	Description
LA	Local Authority
AADT	Average Annual Daily Traffic
GHG	Greenhouse Gas
SGD	Sustainable Development Goal
UN	United Nations
ESA	European Space Agency
DfT	Department for Transport
BEIS	Department for Business, Energy & Industrial Strategy
DESNZ	Department for Energy Security and Net Zero
GSD	Ground Sampling Distance
MAPE	Mean Average Percentage Error
RMSE	Root Mean Square Error
DL	Deep Learning
ANN	Artificial Neural Network

# Chapter 1

## Introduction

### 1.1 Motivation

Sustainable finance encompasses a broad range of activities, products, and stakeholders that strive to align the financial system with global sustainability goals, such as the United Nations' 17 Sustainable Development Goals (SDG's) [1]. However, assessing sustainable finance against these goals can be challenging, due to factors such as regional regulatory differences, limited data availability, and the qualitative nature of some SDGs'.

Satellite imagery has emerged as a promising data source for addressing these challenges. It provides an unbiased and non-invasive source of information that can be standardized and compared across regions. This project leverages satellite imagery to estimate road vehicle greenhouse gas (GHG) emissions by predicting traffic flows from a single satellite image. Transportation is a significant contributor to GHG emissions, accounting for 14% of all direct and indirect emissions. Road transportation is the largest component of this sector, responsible for 73% of total emissions [2].

### 1.2 Objectives

By focusing on road transportation GHG emissions, this project aims to support progress towards the SDG's such as Climate Action and Sustainable Cities and Communities. The objective is to develop a method of transforming a satellite image into road transport Average Annual Daily Traffic (AADT) and GHG emissions. To that end, the following steps are required:

- Satellite image pre-processing and metadata extraction
- Road vehicle object detection and traffic counts prediction
- AADT and GHG emissions prediction

While the scope of this project is limited to the UK, an additional objective is to develop a flexible method that can be adapted to different regions, specifically those

with limited data availability compared to the UK. This is in relation to the aforementioned SGD's, which require a global effort for progress to be most impactful.

## 1.3 Contributions

To achieve the project goals, a two-part end-to-end flexible pipeline is developed.

Firstly, a Deep Learning (DL) object detection model, YOLOv5, is trained and applied to satellite images for automated road vehicle detection. Using true speed data or a live speed estimate and the length of road, we estimate 15-minute traffic counts across four road vehicle classes, categorised by their length. This part is described in Chapter 4.

We then use an Artificial Neural Network (ANN) with one hidden layer to transform the traffic count predictions into Local Authority (LA) Average Annual Daily Traffic (AADT) flow predictions on a per vehicle class basis, this time categorising by vehicle type. Supplementary inputs such as average vehicle speed and the date of satellite image acquisition are also incorporated into the model. This is discussed in Section 5.1.

The AADT predictions can then be used to estimate road transport GHG emissions at the LA level by considering the length of motorway within the LA, fuel consumption, GHG conversion factors, and vehicle licensing statistics, discussed in Section 5.2. Despite the initial pipeline being developed for motorways, we extend the pipeline to A-roads and minor roads. In addition, we provide a way of calculating emissions for regions where vehicle type data is unavailable and perform parametric analysis on the pipeline.

Overall, this project presents a novel pipeline and analysis to estimating road traffic flow from satellite imagery and linking it to road transport GHG emissions. Key contributions are:

- Live speed estimation using a PCA-Based method to predict traffic counts, extending the work by Salehi et al. [3]
- Regional motorway AADT prediction by a subset of 4 vehicle types: cars and taxis, buses and coaches, LGV's and HGV's
- Regional motorway road transport GHG emissions prediction with and without vehicle type data
- Extending regional AADT and emissions prediction to A-roads and minor roads
- Parametric analysis to investigate the effect of parameter values on emissions prediction

By providing new insights and methods in this area, we hope to contribute to the broader effort towards sustainable finance and global sustainability.

# Chapter 2

## Background

In this chapter, we investigate research and data relevant to the project goals, categorised by Section 2.1: Datasets, Section 2.2: Deep Learning (DL) models and Section 2.3: Modelling Methodologies. We then introduce the full pipeline in Section 2.4 and explain how the research findings and datasets are used in relation to the pipeline diagram in Figure 2.3.

### 2.1 Datasets

Project restrictions dictate that datasets should be freely and publicly available. Focus is placed on the UK due to the high availability of data.

#### 2.1.1 Road Transport and Traffic Data

Highways England maintains 15-minute traffic flow datasets for all major roads in England at registered count sites using manual or automatic methods [4]. The dataset includes vehicle counts categorized by vehicle length and average vehicle speed at 15-minute intervals. An API is also available for programmatic access to the data.

Bi-directional AADT data is available at the count site, local authority, and regional levels from the Department for Transport (DfT) [5]. This dataset includes link length between count sites, direction of travel, and vehicle counts categorized by vehicle type, among other information.

Road length statistics [6] are available at the LA and regional level by the DfT. It also categorises road lengths by road type.

Vector data, defined by lines and points, is a natural way to store road network geographies. The DfT uses Shapefiles to store the major road network in England [5].

### 2.1.2 Satellite Imagery Data for Road Transport

For aligning with the project goals, the focus is placed on datasets that include satellite imagery of road vehicles.

VehSat [7] is a large-scale public dataset for vehicle detection in satellite images, published in 2020. It includes 4544 medium-resolution satellite image crops from 8 different areas, with roughly 36,800 vehicle annotations. The images were captured by four different satellites: SkySat, Pleiades, World-View 2, and World-View 3. The dataset covers a wide geographical range, including areas in the USA, Sudan, and China. It does not distinguish between vehicle types and is therefore single-class.

The Satellite Imagery Multi-vehicles Dataset (SIMD) [8] is a multi-class annotated dataset consisting of 5,000 satellite images with roughly 45,000 vehicle objects categorized into 15 classes. The images cover multiple regions in the EU and USA and were acquired from the Google Earth platform.

The Dataset of Object deTection (DOTA) [9] is a large-scale image dataset containing roughly 11,000 images with 1.8 million object instances in 18 classes. The classes related to road transportation are large vehicle and small vehicle. The dataset includes both aerial and satellite imagery at varying resolutions.

xView [10] is another large-scale dataset featuring over 60 classes taken from WorldView-3 satellite images. The parent classes that include road vehicles are Passenger Vehicle and Truck.

Other notable aerial imagery datasets for vehicle object detection that are not taken from satellites include Cars Overhead With Context (COWC) [11], Vehicle Detection in Aerial Imagery (VEDAI) [12], Aerial Image Dataset for Vehicle detection (VAID) [13], and multi-view Vehicle detection in complex Scenarios Using Aerial Images (VSAI) [14].

We provide a summary of the satellite image datasets discussed in Appendix A.

### 2.1.3 Greenhouse Gas Emissions Data for Road Transport

The UK Department for Business, Energy and Industrial Strategy (BEIS) uses vehicle activity datasets to calculate final GHG emissions data [15]. These datasets include vehicle kilometers traveled by different types of vehicles on different types of roads, as well as vehicle characteristics such as age, fuel type, technology, and Euro emission standard.

BEIS maintains a LA and regional GHG emissions dataset from 2005 to 2020 [16]. The dataset is on a yearly scale and has LA GHG Sector and LA GHG Sub-sector granularity. For example, the LA GHG Sector can be filtered to "Transport" and the GHG Sub-sector to "Road." The dataset includes  $N_2O$ ,  $CH_4$ , and  $CO_2$  territorial emissions

(kt CO<sub>2</sub>e), as well as mid-year population (thousands) and area (km<sup>2</sup>) of the LA.

The National Atmospheric Emissions Inventory (NAEI) maintains combined hot exhaust and cold start emissions factors (g/km) for various vehicle types in the UK [17].

BEIS and the Department for Energy Security and Net Zero (DESNZ) have GHG emissions conversion factors [18]. The dataset is published for organisations reporting their GHG emissions, and includes conversion factors by fuel type as well as passenger vehicles type.

The DfT publishes data about fuel consumption, emissions and renewable fuel [19]. The most relevant data is about specific fuel consumption's, which is categorised by vehicle type. In addition, the DfT also publishes data on car registrations by vehicle fuel type [20].

## 2.2 Deep Learning Models

### 2.2.1 Artificial Neural Networks (ANN)

Artificial Neural Networks (ANN's) were developed as a way for a machine to learn complex patterns. Figure 2.1 shows a simple ANN with one hidden layer [21]. The input is in the shape of a tensor, and the nodes represent learnable weights. The output is dependent on the use case, for example in classification problems it may be a probability vector. Each additional hidden layer will add complexity and more expressiveness to the model.

An important characteristic of ANN's compared to other ML models is their ability to use non-linearity. This may be useful if the data has non-linear transformations. For transportation and GHG emission's prediction, this could be day-to-week, week-to-month, and month-to-year traffic count transformations. ANN's are a viable solution when there is a sufficient amount of data available.

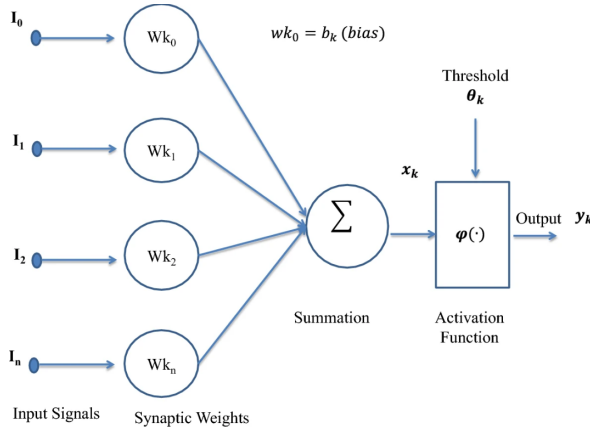


**Figure 2.1:** ANN with one hidden layer [21]

However, there are significant limitations with ANN's when the input is an image. ANN's require many parameters to form the layers of the network when the input is a 2D image because it is considered as a flattened vector. This significantly increases computational complexity when training the network. In addition, ANN's are not able to associate the spatial patterns seen in images as each input is not compared against its neighbours. To this end, Convolutional Neural Networks (CNN's) have been developed.

### **2.2.2 Convolutional Neural Networks (CNN's) for Object Detection**

CNN models for object detection can be roughly divided into two categories: One-stage and two-stage.

Faster R-CNN [22] is a widely used two-stage object detection model. The first stage consists of a region proposal network (RPN), while the second stage is a detection network. Both stages use convolutional layers. For the first stage, a CNN (e.g. VGG) is used as a 'backbone' network with only the layers up until the final convolutional layer. This final layer will therefore output a convolutional feature map to be used as an input into the RPN. The region proposal network slides a window across the convolutional feature map and at each location, classifies a region as either interesting (1) or not interesting (0). To account for potential objects at different scales and aspect ratios, the RPN makes predictions with different sized regions, designated by bounding boxes and often called anchors. The second stage uses a detection network to classify the object and refine its co-ordinate location. The input into the detection network is therefore the regions of interest such that each one can be analysed in more detail, thus improving the accuracy of the final outputs from the model.

For one-stage object detection models, the classification part of the loss function can be modified such that the model attempts a prediction of the object class, as opposed to predicting just an object of interest. Subsequently, the second stage is not needed, thus the predictions of the one-stage object detection models are faster, but less accurate. This is an important consideration when latency is important, for example in real-time applications. For general one-stage object detection models, SoTA level performance has been achieved recently by the YOLO family of models [23].

As an alternative, RetinaNet is a one-stage object detection model that uses a loss function, the focal loss [24], to address class imbalance and up-weight hard training examples. This may make it more suitable for more complicated images with different class sample numbers, such as those seen in satellite imagery.

### 2.2.3 Evaluation Metrics

There are various metrics developed to quantify the performance of DL models, many of which depend on the type of problem being solved. In general, these can be characterised into 2 categories: regression and classification. Regression is used for continuous values, for example AADT and GHG emissions. Classification is for categorical values, for example vehicle type.

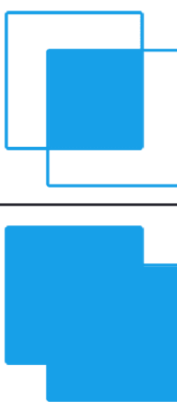
Some of the most popular evaluation metrics for regression tasks include Mean Squared Error (MSE), Mean Average Percentage Error (MAPE), Mean Absolute Error (MAE), etc., all of which have their own advantages and disadvantages.

However, object detection uses a variety of evaluation metrics to compare the performance of computer vision models. At the most fundamental level, evaluating the performance of an object detector is essentially checking if a detection (prediction) is correct or incorrect.

To that end, some metrics can be defined, notably:

- True Positive (TP), a correct detection
- False Positive (FP), an incorrect detection
- False Negative (FN), a missed detection
- True Negative (TN), correctly not detected (e.g. background area)

To calculate these metrics, the Intersection over Union (IoU) value is used, which gives the ratio of intersection and union between 2 boxes, as shown in Figure 2.2. A threshold, between 0 and 1, can then be chosen to convert an IoU value to a metric.

$$\text{IoU} = \frac{\text{Area of Overlap}}{\text{Area of Union}}$$


**Figure 2.2:** Intersection Over Union Illustration [25]

Precision and recall are values which can be calculated from TP, FP and FN, whereby:

$$P = \frac{TP}{TP + FP} \quad (2.1)$$

$$R = \frac{TP}{TP + FN} \quad (2.2)$$

Precision and recall can be plotted as a PR curve by varying the confidence score, a measure of how confident the model is in its detection. The area under this curve is then the Area Under Curve-Precision Recall (AUC-PR), and is often cited as the Average Precision, mAP.

## 2.3 Modelling Methodologies

### 2.3.1 Satellite Imagery Pre-Processing

Before vehicle detection can be performed on a satellite image, some pre-processing steps are required to ensure that each image only contains one side of one road segment. Without these steps, the satellite image would contain road vehicles that are not part of the road segment, for example parked cars along nearby houses. The inclusion of these vehicles would negatively impact results as shown by Jaker Baker [26].

Pan-sharpening [27] is a technique available for some satellite images, such as those taken by WorldView-2/3. It fuses a higher-resolution panchromatic image with a lower-resolution multi-spectral raster image to produce an image with the benefits of both.

Jake Baker [26] uses the specialist software QGIS to mask background pixels to leave only the desired section of road. This can be achieved with the following steps:

- Import the road network shapefile and satellite imagery with geographical metadata
- Project the datasets onto the same coordinate system
- Creating a buffer around the road network that includes only the bi-directional road width
- Intersecting the buffer with the satellite images, and saving the resulting intersected images.

Ganji et al. [28] use a Line Segment Detector (LSD) [29] and road shapefile information to filter for road segments. Road direction information is also extracted from the shapefile, resulting in two distinct road segments representing both directions of the road from the satellite image.

Alternatively, deep learning techniques such as semantic segmentation can be used to automatically extract road segments by masking background pixels. State-of-the-art models include Zhu et al.'s Global Context-aware and Batch independent Network (GCB-Net) [30], and the more readily available DeepLabv3 model [31].

### 2.3.2 Vehicle Detection from Satellite Imagery

Vehicle detection from satellite imagery using DL has recently been dominated by CNN-based object detection models such as YOLO, SSD, RetinaNet, and Faster R-CNN due to their superior performance. However, satellite imagery can pose significant challenges to these models, reducing their accuracy. Road vehicle objects are small compared to other datasets, making them harder to detect. Satellite images often contain complex features that can distract the models. Time of day, weather, and occlusion factors can also degrade accuracy if conditions are unfavorable.

Maity et al. [32] surveyed Faster R-CNN and YOLO-based models for vehicle detection using satellite images and concluded that research could focus on the YOLOv5 version. However, since the paper's publication, a YOLOv8 model has been developed that improves upon YOLOv5.

Kaack et al. [33] compared Faster R-CNN with a ResNet backbone architecture and SSD Inception V2 for truck detection from aerial images. They found that Faster R-CNN had higher performance while SSD Inception V2 had faster inference. However, they used a private dataset for training as the xView dataset was found to be too inaccurate.

Gong et al. [34] implemented a modified YOLOv5 model that uses Swin Transformer Prediction Heads (SPHs) instead of convolutional ones, creating an SPH-YOLOv5 model. This model showed slight improvements on popular datasets such as DOTA [9] when compared to the standard YOLOv5 model.

A method that aims to improve small object detection performance is Slicing Aided Hyper Inference and Fine-tuning (SAHI) [35]. SAHI improves inference detection capability by slicing the image at predetermined lengths, and then doing inference on each slice separately, then combining results. This is especially performance enhancing for satellite imagery due to the small resolution of objects.

### 2.3.3 Traffic Counts

Several methods have been proposed for transforming vehicle detection from satellite/aerial imagery into hourly and/or daily traffic counts. A common feature of successful methods is the separation of the road into its individual directions for analysis, as each direction may have different traffic patterns.

Ganji et al. [28] used a simple artificial neural network (ANN) with one hidden layer to predict daily traffic counts from inputs such as vehicle detection count, road characteristics, and aerial image timestamp. Road characteristics include road width, road type, lane numbers, and speed limit. This represents a relatively complex method due to the level of pre-processing required for each input.

Kaack et al. [33] used a method to convert vehicle detections and road speeds into

traffic counts. Let  $c_I$  be the number of detected vehicles and  $v$  be a constant speed within a defined interval with distance  $d$ . The time taken for a vehicle to travel this distance is  $t_I = \frac{d}{v}$ . From this, daily traffic counts can be approximated as follows:

$$\text{Daily Traffic Count} = c_I \frac{24}{t_I} \quad (2.3)$$

Blattner et al. [36] used a regression tree-based model, CatBoost [37], to predict hourly traffic counts. Additional inputs into the model include weekday and percentage of freeway area covered by clouds. Some section-specific features such as the number of lanes and distance to the next largest city were tested but did not improve model performance and were discarded.

Many of these methods require speed data or an estimation. Salehi et al. [3] developed an automated moving vehicle information extraction model from satellite imagery using the time lag,  $\Delta t$ , in image collection between the MS1 and MS2 sensors on WorldView-2 satellites. This method requires at least MS1 or MS2 band data with the panchromatic band to avoid using live speed data or speed limit data from an alternate source.

### 2.3.4 Annual Average Daily Traffic (AADT) Flow

Ganji et al. [28] used a similar approach to their previous Pattern Recognition Traffic Counts (PRTC) method [38]. This approach uses observations from nearby traffic count sites to estimate AADT, producing an AADT estimate for each road's bidirectional vehicle count detection.

Kaack et al. [33] converted daily traffic counts into AADT by taking into account traffic density factors for hour, day, and month variations ( $f_{h,d,m}$ ). The average daily traffic counts (AADTT) can then be approximated as follows:

$$\text{AADTT} = c_I \frac{24h}{t_I} f_{h,d,m}^{-1} = \text{Daily Traffic Counts} \cdot f_{h,d,m}^{-1} \quad (2.4)$$

Kaack et al. [33] also normalized count values by dividing hourly count data by its mean over a year.

The UK DfT uses a method tailored towards available vehicle activity data, as discussed in the Section 2.1. The method is based off expansion factors, which are used to convert 12 hour manual counts into AADT.

### 2.3.5 Road Transport Greenhouse Gas Emissions

Ganji et al.'s 2020 paper [38] extended their AADT prediction method to also predict GHG emissions at individual roads for multiple years across a large road network. In this paper, segment-level vehicle kilometers traveled (VKT) were multiplied by the corresponding emission factors (in g/veh km) to obtain segment emissions. Road

speed data at different times of day and week was necessary to calculate emission factors, so it was estimated using an artificial neural network (ANN) with inputs believed to correlate with road speed. The resulting output was total emissions on every road segment. To determine the correlations between GHG emissions and AADT and speed, the results were normalized by road length.

The UK Department for Business, Energy & Industrial Strategy uses a method tailored towards available vehicle activity data, discussed in Section 2.1.

### 2.3.6 Evaluation Metrics

Each section of the modeling methodology produces distinct outputs that can be compared to ground truth data, allowing for evaluation of each part of the pipeline.

Vehicle detection from satellite imagery can be evaluated using the metrics discussed in Section 2.2.3.

Predicted traffic counts and AADT results can be evaluated using ground truth data. This can be considered a regression problem, and evaluation metrics such as MAPE and RMSE can be used as described in Section 2.2.3.

However, evaluating AADT is more challenging than evaluating vehicle detection and daily traffic counts due to the differing methods used to calculate it across regions. For example, expansion factors are used to convert manual counts into AADT. For roads without manual counts in the reference year, growth factors are applied to the previous year's AADT. In addition, major and minor road AADTs are calculated differently [39]. These factors should be taken into account when assessing AADT performance using regression evaluation metrics.

Evaluating GHG emissions predictions has similar complications to evaluating AADT. In the UK, the methodology is based on distance traveled by each vehicle, fuel type under different operations, and vehicle- and pollutant-specific emissions factors [40].

Another consideration is that an under-or overestimate of a section will have a cascading impact on the rest of the pipeline. For example, underestimating vehicles detected will likely produce underestimates of traffic counts, which will then affect AADT and GHG emission calculations.

## 2.4 Pipeline Overview

The full pipeline diagram is shown in Figure 2.3. The diagram is split into two parts: 15-minute traffic counts (green) and LA AADT and GHG emissions (blue). This section will summarise the datasets, DL models and modelling methodologies used in the pipeline. The numbers within the diagram boxes correspond to this

section's paragraph numbering. Live speed estimation is dotted to reflect the fact that it is an optional step in the pipeline, as discussed in Section 2.3.3. The variables are lettered, e.g. a), b) etc. for readers to better follow their usage throughout the pipeline. Finally, we include our key metric results from relevant stages in the diagram. Part 1 results are from Chapter 4 and Part 2 results are from Chapter 5.

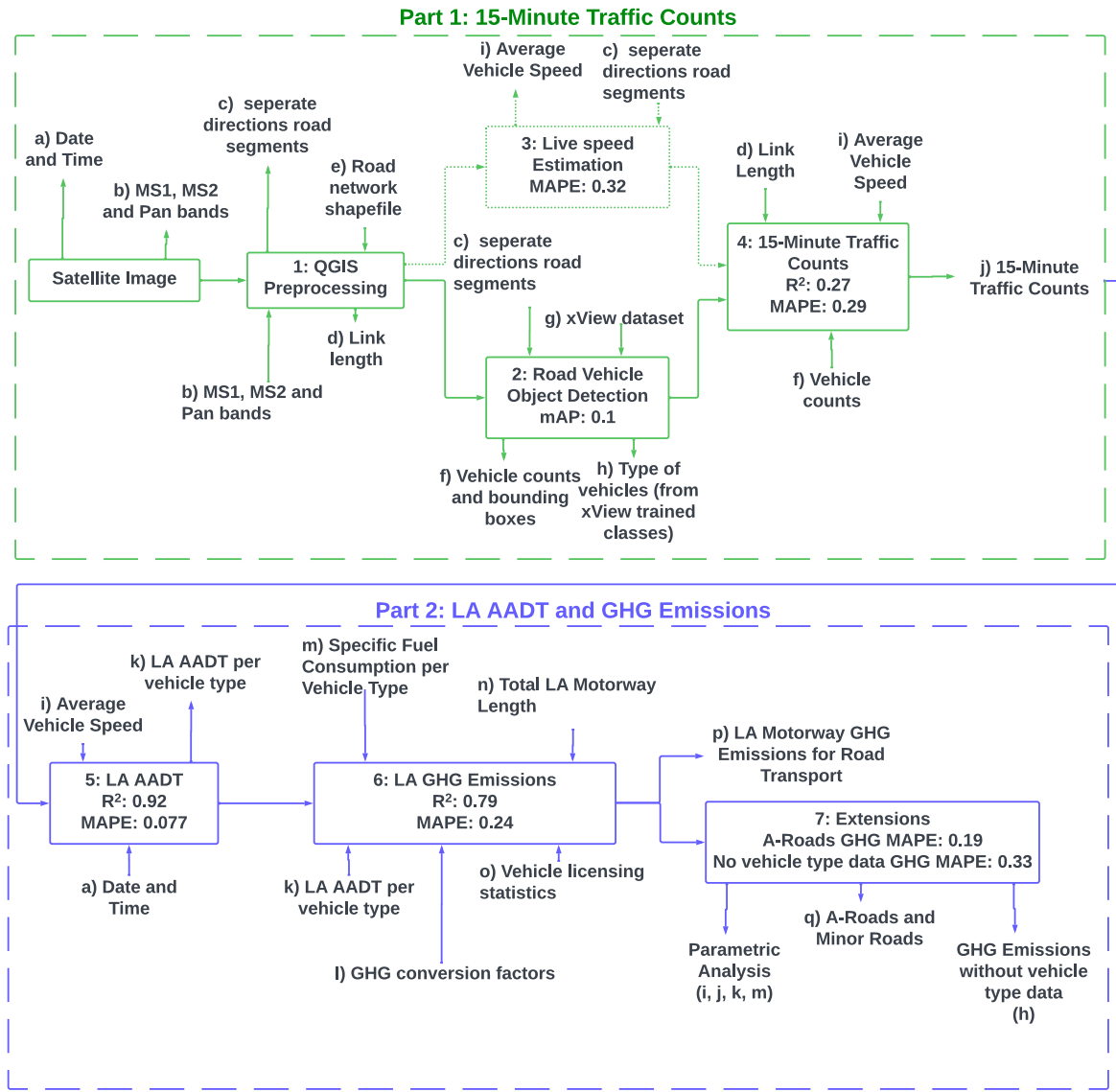


Figure 2.3: Full Pipeline Diagram

#### 2.4.1 Datasets Summary

To summarise, the following datasets are used in the pipeline and referred to in the diagram in Figure 2.3 via the numbering and lettering scheme.

- 1: The road network dataset in shapefile format is used for its geographical information and QGIS compatibility during satellite imagery pre-processing. This is variable e).

5: The Highways England traffic count dataset [4] is used as input variables for AADT training and prediction due to its convenient API access and rich data. The bi-directional AADT at the LA level dataset [5] is used as the ground truth for vehicle type AADT values. These are variables i) and j).

2: The xView dataset [10] is chosen as the main dataset for training the vehicle object detection model. It includes WorldView-2 and 3 satellite images, commonly used by the European Space Agency (ESA) and required for live speed estimation. Fine-tuning on the VehSat dataset [7] did not improve model performance, likely due to its lower resolution compared to xView. This is variable g).

6: The BEIS LA GHG emissions dataset [16] is used as the ground truth for emissions evaluation, for comparison to the output variables p) and q). It provides flexible granularity of road emissions at the LA level. In addition, the UK GHG conversion factors [18], fuel consumption [19] and vehicle license [20] are used for emissions calculation. These are variables l), m) and o) respectively. Finally, we use n) total motorway length [6] to scale emissions results to the LA level.

These datasets are further explored to suit the project goals in Chapter 3.

#### **2.4.2 DL Models Summary**

To summarise, the following DL models are used in the pipeline and referred to in the diagram in Figure 2.3 via the numbering and lettering scheme.

2: For vehicle object detection from satellite imagery, a CNN-based model is chosen. While Transformer-based models show promise and have some advantages over CNN-based models, they also have disadvantages such as requiring more data to achieve comparable results and having less support due to their more recent development.

5: An artificial neural network (ANN) is used to predict AADT. ANN's are a suitable choice due to the large traffic count dataset provided by Highways England [4]. Data-driven approaches can generalize well by minimizing assumptions and adapting to changing patterns faster and more robustly than less data-driven methods. ANN's can also learn non-linear functions, potentially improving performance by capturing more complex data distributions compared to linear methods such as regression.

#### **2.4.3 Modelling Summary**

In summary, the following models are used in the pipeline and referred to in the diagram in Figure 2.3 via the numbering and lettering scheme.

- 1: QGIS pre-processing was chosen after conducting qualitative tests using other methods discussed in Section 2.3.1. Deep learning segmentation methods to automatically extract road pixels showed unsatisfactory performance on test images from public satellite image datasets. As the project only considers major roads in the UK, QGIS can utilize shapefile-format datasets from Section 2.1 for simple and accurate pre-processing. The input at this stage is the raw satellite image bands, variable b). The outputs are c) separate directions road segments and d) link length.
- 2: The YOLOv5 model is used as the baseline model for vehicle detection due to its support for training and optimization for small objects such as those in satellite images, for example the SAHI framework [35] which is used during inference. The input to the trained model is c) separate directions road segments and the outputs are f) vehicle counts and bounding boxes and h) xView vehicle classification.
- 3: Live speed estimation provides pipeline flexibility by negating the requirement of historical speed data. We extend the PCA-based estimation method developed by Salehi et al. [3], which uses the lag between MS1 and MS2 images in WorldView-2 and 3 satellites. The input at this stage is c) separate directions road segments and the output is i) average vehicle speed.
- 4: For traffic count prediction, a method similar to that used by Kaak et al. [33] and Jake Baker [26] is used, but modified to estimate 15-minute traffic counts for compatibility with the Highways England dataset [4]. Speed is required as an input variable due to its significant improvement in performance [26]. We use inputs d) link length, f) vehicle counts and i) average vehicle speed to predict j) 15-minute traffic counts.
- 5: AADT prediction uses a simplification of Ganji et al.'s method [28]. Instead of explicitly calculating transformations, an ANN is used to learn the transformations and predict AADT directly. AADT is predicted per vehicle type as well as for all motor vehicles, i.e. in a multi-output regression format. We use a) date and time, j) 15-minute traffic counts and i) average vehicle speed to predict k) LA AADT per vehicle type.
- 6: GHG emissions estimation uses l) GHG fuel conversion factors, k) predicted AADT values, m) fuel consumption per vehicle type, o) vehicle licensing data and n) total motorway length to calculate emissions for each vehicle type in an LA. Total emissions are then found by summing across all vehicle types for p) LA motorway GHG emissions for road transport.
- 7: We extend the base pipeline to provide flexibility and additional insights and contributions in relation to the project goals, Section 1.2. These include parametric analysis on variables, extending emissions prediction to A-roads and minor roads as well as predicting emissions when AADT by vehicle type data is not available. The lettering in brackets indicates what variables are used/analysed for extension.

# Chapter 3

## Exploratory Data Analysis

### 3.1 Motorway Road Transport

#### 3.1.1 15-Minute Traffic Counts

The Highways England dataset [4], mentioned in Section 2.1, provides 15-minute traffic counts for the years 2005-2021 across the UK major road network. These traffic counts are performed by unique count sites that vary in several ways: some are permanent while others are temporary, some are automatic while others are manual, etc. Each count site monitors only one side of the road, so count sites can generally be grouped into pairs with names that have the suffix "A/B" or differ by one number to denote them as a pair. Table 3.1.1 shows the features recorded at each count site along with a brief description. All data types are integers.

**Table 3.1:** 15-Minute Traffic Count Dataset Features

Feature	Description
Hour of Day	The hour of the day when the traffic count is made
Day of Week	The day of the week when the traffic count is made
Month of Year	The month of the year when the traffic count is made
Live Speed	Live speed
Small vehicle count	Number of vehicles between 0-520cm
Medium vehicle count	Number of vehicles between 521-660cm
Large vehicle count	Number of vehicles between 661-1160cm
Very Large vehicle count	Number of vehicles over 1160cm
Total Vehicles	Total number of vehicles

### 3.1.2 Local Authority AADT

The LA AADT bi-directional dataset [5] is maintained for each local authority for all major and minor roads. Each local authority dataset has the count point ID, as explored in Section 3.1.1, and year as the primary key. Notable features and their descriptions are shown in Table 3.1.2.

**Table 3.2:** Local Authority AADT by direction Dataset Features

Feature	Description	Data Type
Year	The year when the traffic count is made	Integer
Road Name	The name of the road	String
Link Length (km)	The length of the road link in kilometers	Float
Estimation Method	The method used to estimate traffic counts	String (Automatic or Manual)
Cars and Taxis	Number of cars and taxis	Integer
Buses and Coaches	Number of buses and coaches	Integer
LGVs	Number of light goods vehicles	Integer
HGVs	Number of heavy goods vehicles	Integer
All motor vehicles AADT	Total number of motor vehicles	Integer

To analyze the distribution of the data, a subset of LAs were chosen based on the criteria described in Section 4.1. Figure 3.1 shows the LA AADT's per year from 2005 to 2020, calculated using the maximum value over all count sites situated within the LA.

Figure 3.2 shows histograms of count site AADT values for the Havering LA as an example for the 2017 and 2018 years. Appendix B shows the remaining chosen LAs. It can be seen that LA AADT values showed an increase from 2017 to 2018, proving the upward trend known to exist for traffic data.

Motorway Maximum LA AADT per year for each LA

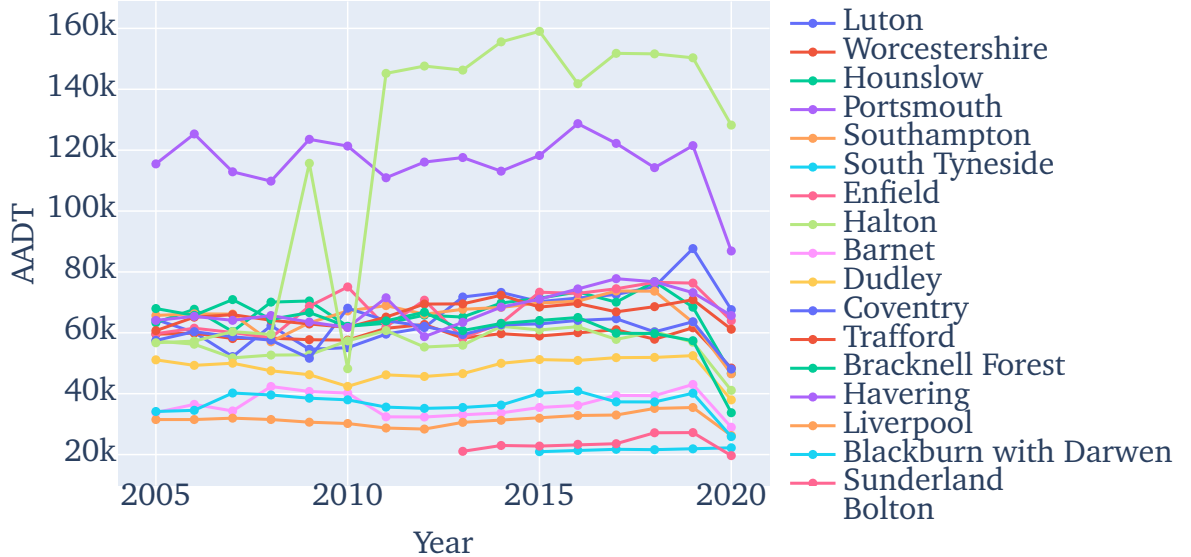


Figure 3.1: LA Maximum AADT's per year

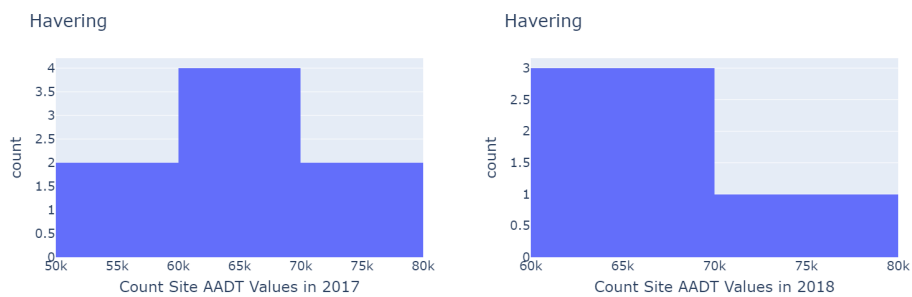


Figure 3.2: LA AADT Count Site Havering Histograms

The LA AADT by direction data [5] also produces AADT's by vehicle type as well as total AADT. The vehicle types included are cars and taxis, buses and coaches, LGV's, and HGVs. Figure 3.3 shows maximum values per year across count sites for each vehicle type as a stacked bar chart for the Havering LA. The bar charts for the rest of the chosen LA's is shown in Appendix C. It was evident across all chosen LA's that cars and taxis make up the majority of vehicles, around 70%.

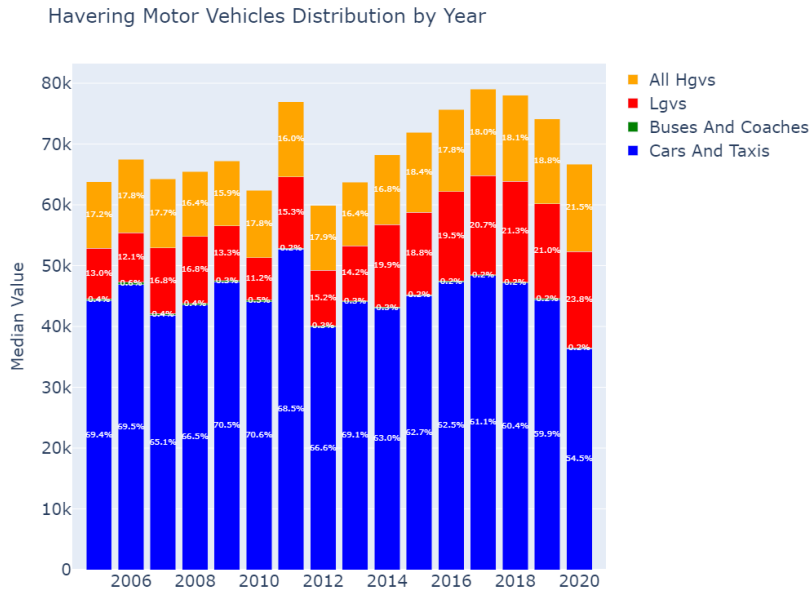


Figure 3.3: Havering LA AADT by Vehicle Type

Overall, AADT is relatively stable through the years, with some LA's experiencing slight increases or decreases. 2020 is a notable year as every LA's AADT decreased significantly due to the impact of COVID-19 on travel. This suggests that 2020 may be treated as an outlier.

## 3.2 Satellite Imagery for Road Transport

### 3.2.1 Specifications

Satellite data often comes with multiple imagery's, notably Panchromatic (PAN) and Multi-spectral (MS). The datasets are generally in raster format unless specified otherwise. Raster format uses pixels to store image data, where each pixels corresponds to a spatial resolution. Raster data can also contain geographical information as metadata, for example the latitude and longitude of the center or the area vertices of the image.

### 3.2.2 xView for Model Training

The xView dataset is designed for various tasks and so includes classes ranging from damaged buildings to helicopters. For road transport, the following parent classes are of interest: Passenger vehicle and truck. The images are pan-sharpened and ortho-rectified.

Figure 3.4 shows a training example with bounding boxes rendered visually. The bounding boxes around vehicles are of most interest to this project.

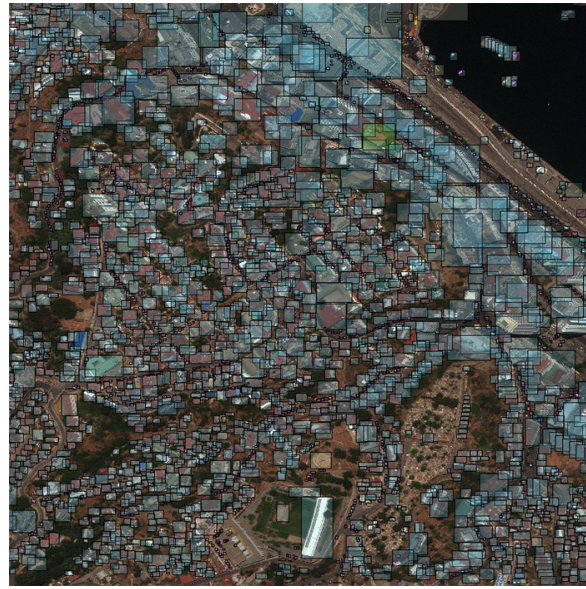


**Figure 3.4:** xView Training Set Example

### 3.2.3 European Space Imaging

In this section, we focus on the WorldView-2 and WorldView-3 satellites, which provide Panchromatic (RGB), Multi-spectral 1 (B,G,R,NIR1), and Multi-spectral 2 (C,Y,RE,NIR2) imagery across 8 separate bands. To explore the available archive data, we utilized the European Space Imaging library GUI [41].

This interface allows for the definition of Areas of Interest (AOIs) using polygons and enables automatic viewing of past images captured within the specified AOI. Figure 3.5 illustrates an AOI drawn around the Luton LA and the corresponding archive data displayed in chronological order. The GUI does not display images at full resolution.

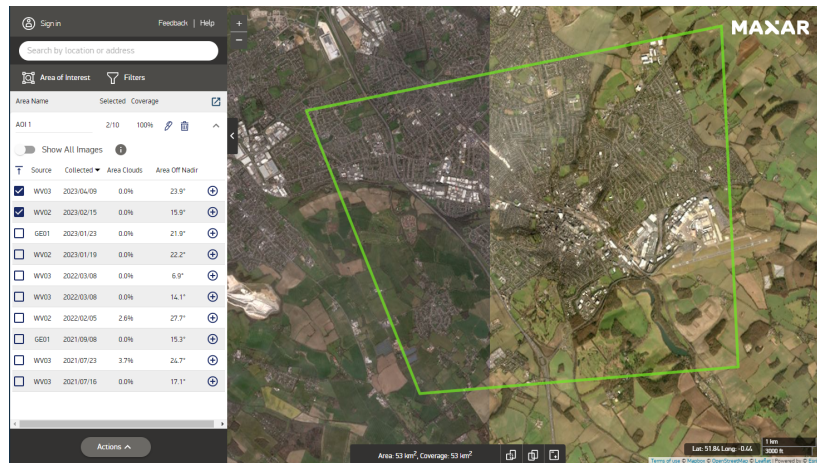


**Figure 3.5:** EU Space Imaging GUI

## 3.3 Motorway GHG Emissions

### 3.3.1 Local Authority GHG Emissions

The LA GHG emissions data [16] is reported annually and provides values per road type. Key features and their descriptions are presented in Table 3.3.1.

**Table 3.3:** Features of Local Authority GHG Emissions Data

Feature	Description	Data Type
Local Authority	The local authority responsible for the road	String
Calendar Year	The year in which the data was recorded	Year
LA GHG Sector and Sub-Sector	The sector and sub-sector of GHG emissions	String
Greenhouse gas	The type of greenhouse gas emitted	String
Territorial emissions (kt CO <sub>2</sub> e)	The total territorial emissions in kilotons of CO <sub>2</sub> equivalent	Float
Mid-year population (thousands)	The mid-year population of the local authority in thousands	Integer
Area (km <sup>2</sup> )	The area of the local authority in square kilometers	Integer

To calculate the total annual territorial emissions for motorways within a specific LA, the data is first filtered to include only motorways. The Territorial emissions (kt CO<sub>2</sub>e) field, which includes N<sub>2</sub>O, CH<sub>4</sub>, and CO<sub>2</sub>, is then summed to produce a total value.

Figure 3.6 displays the annual territorial emissions (kt CO<sub>2</sub>e) for a subset of LAs. Similar to AADT, the values remain relatively stable over time, with a notable decrease observed in 2020.

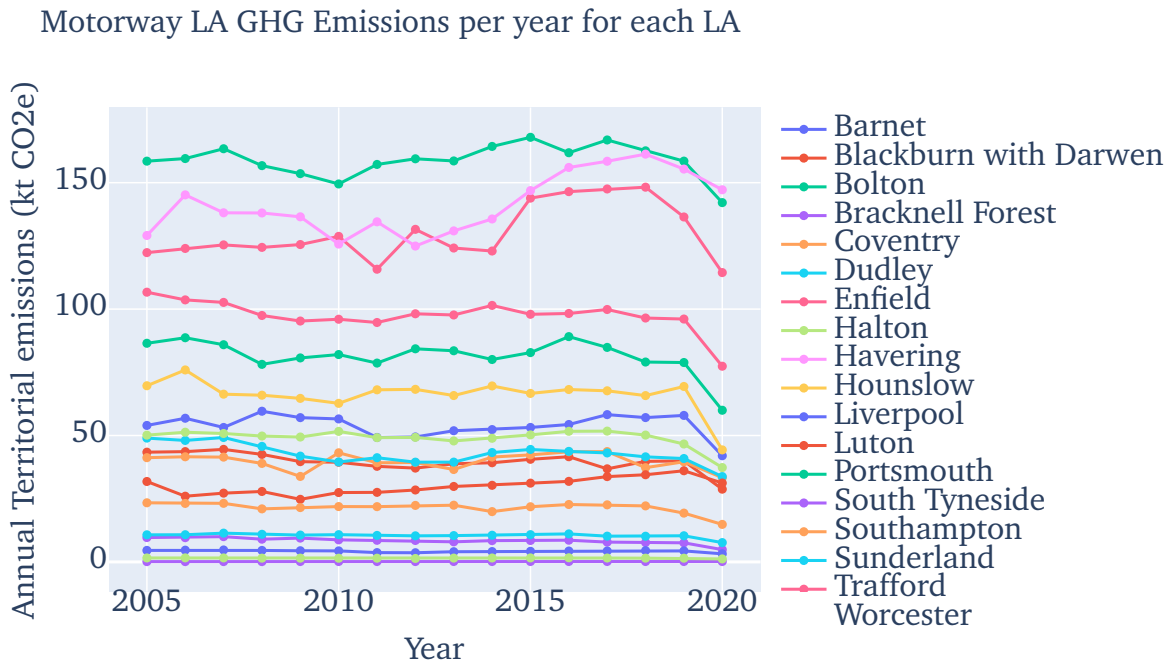


**Figure 3.6:** LA GHG Emissions per year

## 3.4 Motorways Summary

In summary, Figure 3.7 presents a scatter plot of LA AADT and GHG emissions, with each marker representing a single year. An Ordinary Least Squares (OLS) line of best fit is also included to illustrate the overall trend. As anticipated, there is a positive correlation between AADT and GHG emissions.

It is also worth noting that some LA's exhibit values that deviate significantly from the OLS line. For instance, Bracknell Forest (red) has high AADT but low GHG emissions, while Bolton (pink) has medium AADT but very high GHG emissions. These discrepancies may be attributed to other factors not considered in this analysis or a limitation in the modelling or assumptions.

A common pattern observed across local authorities is the presence of an outlier for the year 2020, indicated by a single marker located towards the bottom left corner of the plot relative to the other markers for that local authority. Finally, it should be noted that the LA's analysed in this section all share common characteristics as defined in Section 4.1. Thus, the reliability of the analysis is limited to LA's that follow the same characteristics.

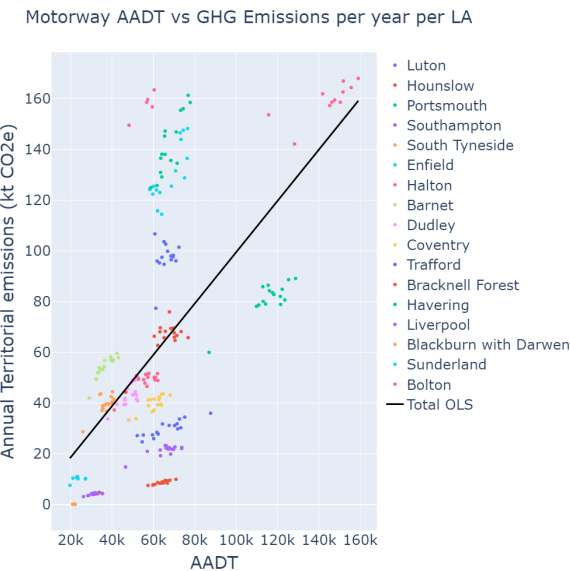
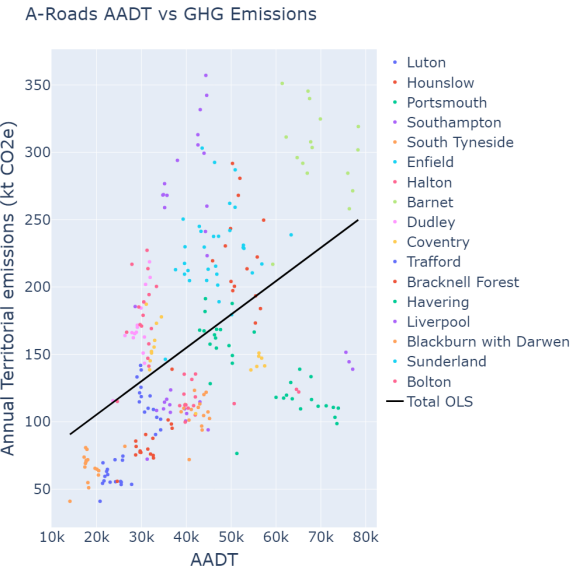


**Figure 3.7:** Motorway LA AADT and GHG Emissions Scatter Plot

### 3.5 Extension to Other Road Types

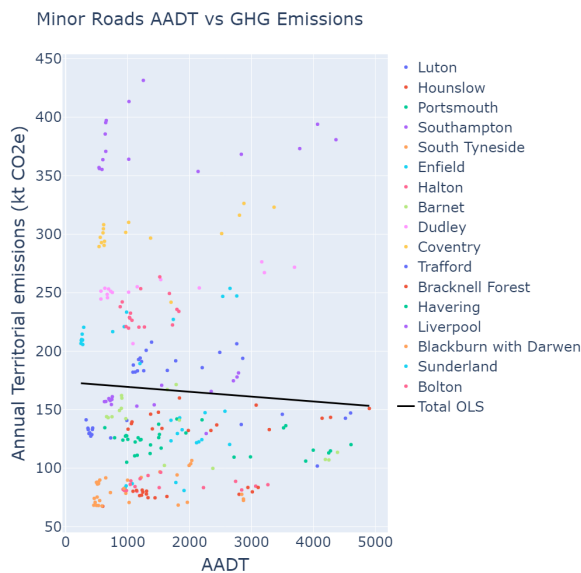
In this section, we extend our exploratory data analysis to A-roads and minor roads within the same subset of LA's as for motorways analysis.

Figure 3.8 illustrates the joint plot of LA AADT and GHG emissions for A-roads, with each marker representing a single year and the OLS line of best fit included. For AADT, the figure reveals a higher level of fluctuation compared to motorways; however, there is generally consistency across years, with LA's such as Southampton (purple) being considered outliers in their distribution. For GHG emissions, interestingly, the graph shows a gradual decrease in emissions over time, which is not observed for motorways. Overall, the scatter plot reveals a positive correlation between AADT and GHG emissions, similar to that observed for motorways



**Figure 3.8:** LA A-Roads AADT vs GHG Emissions Scatter Plot

Figure 3.9 shows the joint plot of median LA AADT and GHG emissions for minor roads, where each marker indicates a single year and an OLS line of best fit. The median value is chosen for exploration as minor roads are subject to much higher variability in traffic compared to major roads (A-roads and motorways), thus the median provides a level of robustness against outliers that the maximum value doesn't. GHG emissions per year are relatively constant. Overall, the scatter plot shows no correlations, a significant difference compared to motorways and A-roads. This would suggest that minor roads would produce significantly worse results than motorway or A-roads.



**Figure 3.9:** LA Minor Roads AADT vs GHG Emissions Scatter Plot

Appendices D and E show the A-roads and minor roads AADT and GHG emissions per year on separate diagrams, respectively. In addition, Appendix F shows the

Havering vehicle type distributions per year for A-Roads and minor roads. A-roads show similar vehicle distributions to motorways, while minor roads show a significant decrease (by around a factor of 9) in median vehicle AADT from 2009 to 2010, where it remained steady until 2020, where it increased back to 2009 levels.

# Chapter 4

## Implementation of Motorway Traffic Counts

In this chapter, we present Part 1: 15-Minute Traffic Counts of the proposed pipeline outlined in Section 2.4, and diagram shown in Figure 2.3.

The input to the pipeline is a satellite image covering the chosen count sites. If vehicle speed estimation is required, the 8-band satellite image is used. The image acquisition date and time are extracted for use in AADT prediction. The criteria for choosing count sites, image acquisition areas, and image requirements are discussed in Section 4.1.

QGIS pre-processing is used to convert the satellite image into a Pan-sharpened image with separate directions and a masked background. The rest of the pipeline considers only one direction, as it is repeated for the other direction. The pre-processing steps are described in Section 4.2.

The processed Pan-sharpened image is then used for vehicle object detection. The output of the deep learning model on each satellite image includes bounding box values and vehicle class predictions for each detected vehicle in the image. These values are used to categorize vehicles by size for use in AADT prediction. Road vehicle object detection is discussed in Section 4.3.

Live speed estimation can be performed using principal component analysis (PCA) on the time-lag between MS bands of the satellite image, based on Salehi et al. [3]. If historical speed data is available, live speeds can be taken from the road transport dataset as described in Section 2.1. Live speed estimation is investigated in Section 4.4.

An estimation of 15-minute traffic counts is then made by using the output of the object detection model, the road length segment of the processed satellite image, and speed data. 15-minute traffic count estimations are described in Section 4.5.

## 4.1 Chosen Count Sites

Due to constraints on satellite image acquisition by the European Space Agency, we are limited to acquiring a maximum of 125km<sup>2</sup> of land area, with each area of interest (defined by a polygon) being at least 25km<sup>2</sup>. As a result, we have chosen 5 count site pairs to use in the pipeline, each residing in a different LA. These constraints and their reasoning are summarized in Table 4.1.

**Table 4.1:** Choosing UK Site Constraints

Constraint	Reasoning
Minimize LA km <sup>2</sup>	Simplifies LA selection and increases likelihood of matching other constraints
Avoid big cities and towns	Complicates data pre-processing and evaluation
Only one motorway through LA	The pipeline only considers motorway GHG emissions and image acquisition only covers one motorway per LA
<90% missing data on count site	ANN AADT training requires sufficient count site data
Bidirectional traffic count site data	The pipeline considers both road directions separately
Traffic count site not within a junction	Traffic count methods cannot consider vehicles leaving/joining at a junction.

## 4.2 WV-2 Satellite Image Pre-Processing

The QGIS pre-processing method is chosen to convert the raw satellite images of the count sites into Pan-sharpened, masked images that only contain one side of the road around the count site. Figure 4.1 shows the Havering MS1 band satellite image before pre-processing. Appendix G shows the rest of the chosen LA's satellite images before pre-processing.

Thus, each image input will produce 2 masked output images for each direction. The following steps describe the data pre-processing:

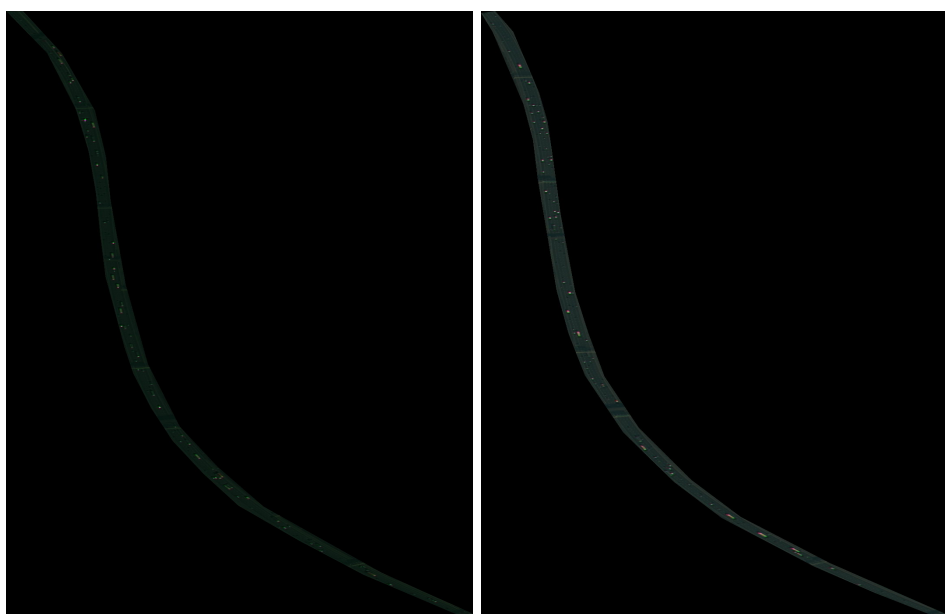
1. Load raw image and import road network
2. Project the datasets onto the same co-ordinate system
3. Create a Pan-Sharpened image using the RGB bands of MS1 and grayscale Pan images.
4. Create a buffer around the road network that includes only the bi-directional road width.

5. Intersect the buffer with the satellite images
6. Save the resulting intersected images



**Figure 4.1:** Havering MS1 WV-2 Satellite Image

The length of buffer distances is inspired by Jake Baker [26] and depends on the number of lanes: 7m for 2 lanes, 11m for 3 lanes, and 14m for 4 lanes. In addition, longer link lengths have been shown to produce more stable results due to averaging effects. As a result, clipped images are maximized in length subject to these criteria. Figure 4.2 shows the final processed image for Havering count sites M1/2557A and M1/2557B, and a zoomed version for clarity. Appendix H shows the processed images for the other chosen LA's.



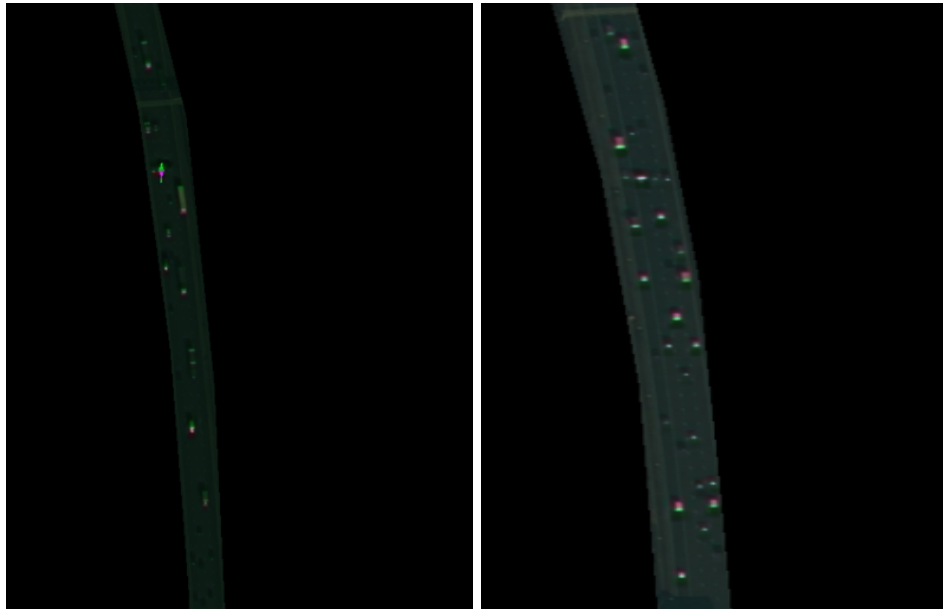


**Figure 4.2:** Havering M25/5790A and M25/5790B WV-2 Processed Images

For other parts of the pipeline, the acquisition date and time of the WV-2 images are necessary. Table 4.2 shows these values for each LA. The dates are constrained to be within 2018 as this is the test year.

**Table 4.2:** LA WV-2 Image Acquisition Date and Time

Local Authority	Date (DD/MM/YYYY)	Time (hh:mm)
Blackburn with Darwen	24/02/2018	11:23
Havering	16/02/2018	11:19
Luton	18/11/2018	11:08
Hounslow	18/11/2018	11:09
Trafford	24/02/2018	11:23

## 4.3 Road Vehicle Object Detection

### 4.3.1 Model Training and Validation

For road vehicle object detection, we use the YOLOv5 medium-sized model trained on the road vehicle classes of the xView dataset [10]. Training uses the Ultralytics [42] and small object detection [35] frameworks.

A significant change made to the YOLOv5 Ultralytics default configuration is the incorporation of the focal loss function from RetinaNet, discussed in Section 2.2.2. This is due to the class imbalances in the xView dataset and complex background with small objects.

Figure 4.3 shows a training example batch with data augmentation. As discussed, only the road vehicle classes are used. Appendix I shows the full training results.

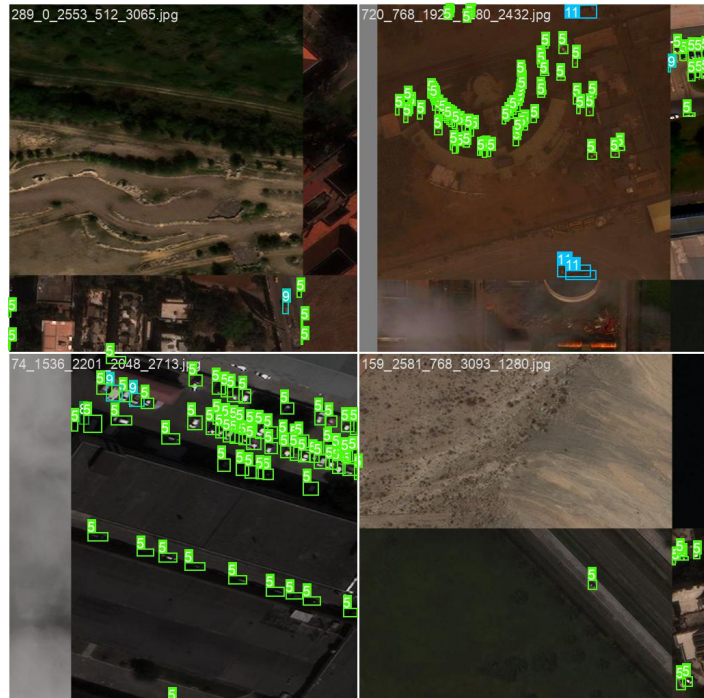


**Figure 4.3:** xView road vehicles example training batch

### 4.3.2 Model Inference

Figure 4.4 shows a zoomed in section of the inference results on the Havering M25/5790A count site from the trained YOLOv5 model using SAHI: Slicing Aided Hyper Inference framework [35]. The numbers depicted represent the confidence of the model's predictions. The confidence threshold is set very low (approximately 0.005) as trial and error has shown that the model performs best at low confidence thresholds.

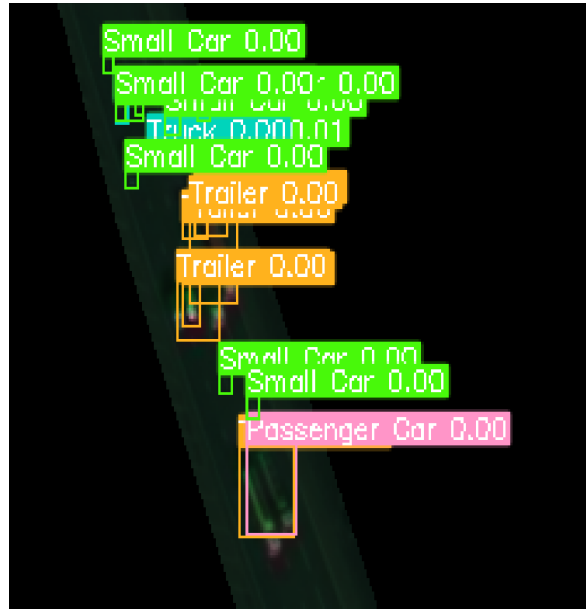


**Figure 4.4:** Havering Object Detection Zoomed Section

The inference output for each detected vehicle and its usage in the pipeline is as follows:

- bounding box values ( $x\_min$ ,  $x\_max$ ,  $y\_min$ ,  $y\_max$ ) for calculating vehicle length for compatibility with the UK traffic counts dataset [4]
- xView vehicle classification for use when AADT vehicle type data isn't available. The mapping table and implementation are described in Section 5.3.1

## 4.4 Live Speed Estimation

Historical average speed data at the time of image acquisition is treated as ground truth values and should be used for optimal results in the rest of the pipeline, if possible. They are taken from the 15-minute traffic count that reside within the image acquisition time. Table 4.3 shows the ground truth speeds.

**Table 4.3:** Live Average Speed Values for each Count Site

Local Authority	Site 1: Speed (mph)	Site 2: Speed (mph)
Blackburn with Darwen	30361033: 66	30361032: 65
Havering	M25/5790A: 63	M25/5790B: 63
Luton	M1/2557A: 65	M1/2557B: 63
Hounslow	M4/2188A: 65	M4/2188B: 59
Trafford	M60/9083A: 67	M60/9086B: 65

#### 4.4.1 PCA-Based Method

In this section, we extend the PCA-based by Salehi et al. [3]. We use properties of WorldView-2/3 satellite images, specifically the time lag between MS1 and MS2 bands, to predict average road vehicle speed. This time lag, approximately 0.13 seconds, allows us to compare the images produced from the MS1 and MS2 bands and infer average vehicle speed using the following method:

1. Stack the MS1 and MS2 images
2. Apply principal component analysis (PCA) to the stacked images
3. Choose the fourth principal component (PC4) as it best represents changes in vehicle location (from Salehi et al. [3])
4. Calculate the centroids of moving vehicles in MS1 and MS2 separately
5. Determine the ground position of centroids before and after the time lag, giving  $(X_1, Y_1)$  and  $(X_2, Y_2)$
6. Calculate the displacement vector  $\Delta P = \sqrt{\Delta X^2 + \Delta Y^2}$
7. Calculate speed  $v = \frac{\Delta P}{\Delta t}$

Where  $\Delta t$  is the time lag and  $\Delta P$  is the average distance traveled by road vehicles during that time lag.

The fourth principal component reconstruction image is referred to as the PC change image. In this image, each moving vehicle is represented by two neighboring objects with very dark and very bright gray values. This allows for the detection of vehicles before and after the time lag.

To locate these dark and bright objects, we specify an area, compactness and rectangular shape criterion. This is an extension to the criteria used by Salehi et al. [3], where they used only compactness. Potential objects above a threshold for these criteria are identified as road vehicles. The threshold values are hyper-parameters that are optimized by visual inspection on a subset of randomly chosen count site PC change images.

Figure 4.5 shows a zoomed in section of the PC change image for Havering M25/5790A (left) as well as the detected vehicle centroids, indicated by red dots (right).

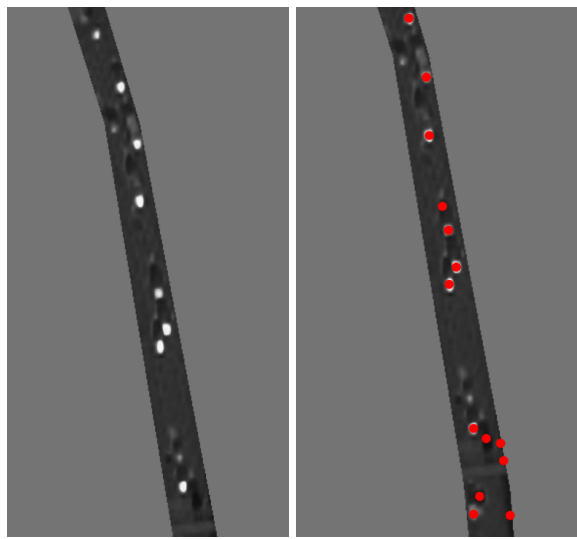


**Figure 4.5:** Zoomed Section of Havering PC Change Image (left) and Vehicle Centroids Detection (Right)

#### 4.4.2 Results

Figure 4.6 shows the MAPE of live speed estimation against historical speeds, as a bar chart. Where a count site shows an MAPE of 1.0, this means no vehicles were paired, i.e. a bright and dark spot were not found within a threshold value of each other. This threshold value corresponds to the maximum distance a car could travel at 70mph in the time lag. Visual inspection of the images show that they all contain vehicles and so at least one vehicle pair should be found. Thus, this represents a failed stage in the live speed estimation method.

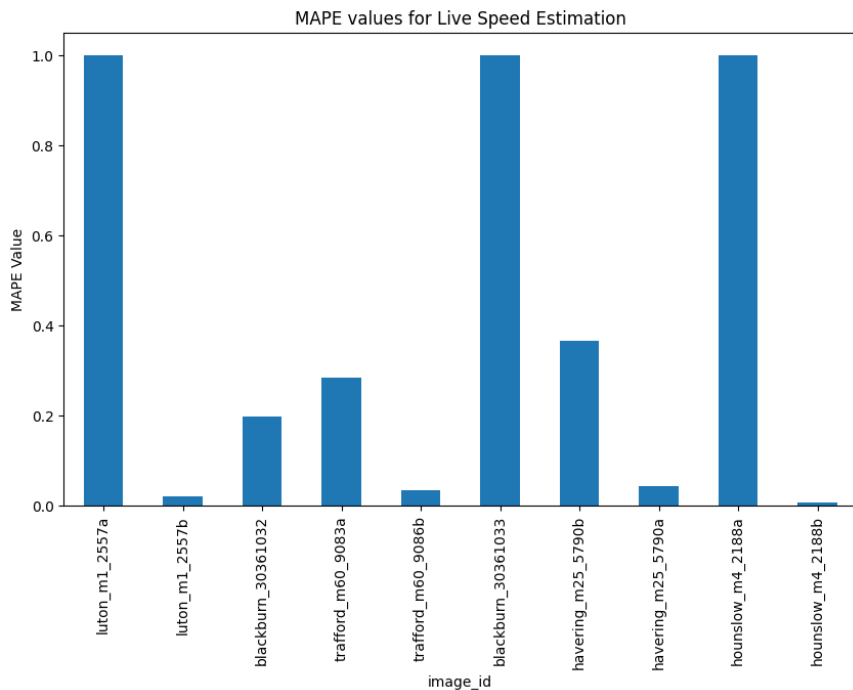


**Figure 4.6:** Live Speed Estimation MAPE Bar Chart

## 4.5 15-Minute Traffic Counts

Traffic count estimates are calculated using vehicle speeds, the detected number of road vehicles, and the link length (km). Recall the formula used by Kaack et al. [33] and discussed in Section 2.3.3:

$$N_{i15} = 15 \frac{vN_i}{l} \quad (4.1)$$

The link length  $l$  is the length of road within the masked image,  $N_i$  is the number of vehicles detected by vehicle length, and  $v$  is the average speed. For number of vehicles detected, we map bounding boxes to the UK compatible vehicle traffic counts, which are categorised by vehicle length as shown in Table 3.1.1. The mapping is done using the following method:

1. Calculate length of vehicle in pixels using bounding box corners
2. Convert pixel length to centimetre length with known Ground Sampling Distance (GSD)
3. Categorise vehicle by vehicle length in cm

### 4.5.1 Results

Table 4.4 shows the RMSE and MAPE error metrics for each LA when using historical speed data. The last row of the table is an average score across the count sites. Figure 4.7 shows the scatter plot of predicted vs true 15-minute traffic counts. The  $R^2$  coefficient is 0.27.

**Table 4.4:** 15 Minute Traffic Counts Results Table

LA Count Site	RMSE	MAPE
Blackburn 30361032	57	0.122
30361033	263	0.47
Luton M1/2557A	557	0.50
M1/2557B	200.3	0.17
Havering M25/5790A	604	0.51
M25/5790B	3.4	0.003
Hounslow M4/2188A	320	0.42
M4/2188B	24.5	0.031
Trafford M60/9083A	576	0.61
M60/9086B	54.9	0.063
AVERAGE	266	0.29



Figure 4.7: 15 Minute Traffic Count True vs Predicted Values Scatter Plot

## 4.6 Evaluation

This section will evaluate the methods to produce 15-minute traffic counts from a processed satellite image.

The YOLOv5 model, trained on the xView road vehicle dataset, is able to perform inference on road lengths of varying shapes and sizes due to performance enhancements implemented, such as SAHI [35]. Thus, it is unlikely that a Transformer-based model would significantly improve results for the goals of this pipeline. A hyper-parameter that can significantly affect results is the threshold confidence value. A lower threshold value can overestimate the number of detected vehicles, for example. The YOLOv5 model has not over-fitted from the xView dataset and so results would likely improve from further model training, however this project is limited due to computational and time restrictions.

Live speed estimation can produce MAPE values of less than 0.05, for example the Luton count site M1/2557A. However, it can also fail to produce an estimate for some images. A possible reason and disadvantage for PCA-based speed estimation is the level of hyper-parameter tuning. This will be a significant consideration as the pipeline is scaled in order to meet the project goals. In the original paper [3], only one image was used, thus parameter tuning was simpler. Figure 4.8 shows the

MAPE comparison on 15-minute traffic count predictions when using ground truth speed data vs the PCA-based estimation.

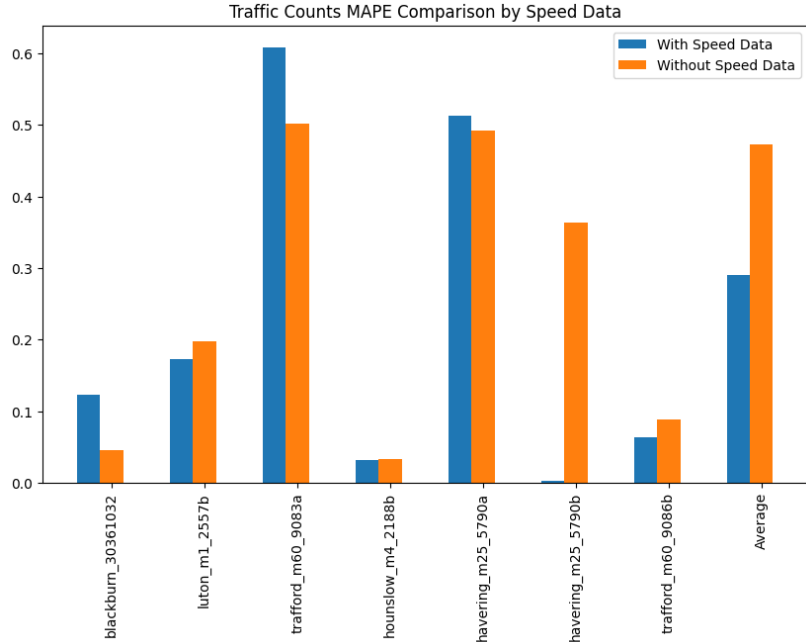


**Figure 4.8:** Speed Data 15-Minute Traffic Count MAPE Comparison

A limitation of this comparison is that there was not a wide range of true speeds from the ground truth data, the lowest being 59mph and the highest was 67mph, thus the method isn't tested at lower speeds. Another limitation of the MAPE comparison is that in general, speed estimation overestimated true speeds. As object detection generally under-estimates by design, the overestimate in speed compensates for this under-estimation slightly, thus the MAPE values seen are likely more optimistic for without speed data than in reality.

Overall, the pipeline to produce 15-minute traffic counts from a single satellite image builds upon previous research in this area. However, the method of PCA-based live speed estimation is novel, and represents an advancement towards the project goals where speed data may not be available.

# Chapter 5

## Implementation of LA AADT and GHG Emissions

In this chapter, we present Part 2: LA AADT and GHG Emissions of the proposed pipeline outlined in Section 2.4, and diagram shown in Figure 2.3.

At this stage, the input variables can be used on the pre-trained ANN for AADT prediction. Historical speed data is used in this chapter instead of the PCA-based estimation for optimal results. The output is then an AADT prediction at the LA level for all motor vehicles, as well as cars and taxis, buses and coaches, LGV's, and HGV's separately. This implementation is described in Section 5.1.

GHG emissions are then modeled using the AADT prediction's and external information, as discussed in Section 2.4. The GHG emissions prediction is scaled for the total length of the motorway within the local authority for comparison with ground truth data from the UK government. This implementation is described in Section 5.2.

Finally, we present various extensions and flexibility to the pipeline with the following additions:

- Section 5.3.1: Estimating vehicle type data for regions where vehicle type data is not available.
- Section 5.4: Analysis of the effect of varying parameters on LA AADT and emissions predictions
- Section 5.5: Producing estimates of LA AADT and GHG emissions for other road types, specifically A-roads and minor roads.

### 5.1 Motorway LA AADT

#### 5.1.1 ANN Traffic Data Pre-Processing

The traffic count dataset [4] is first pre-processed to be suitable for input into an ANN, where the inputs and description are discussed in Table 3.1.1. This creates

one dataset per count site.

Each row in the dataset for ANN AADT Predictions is treated as a different data-point, thus assuming independent and identically distributed data. A min-max standardisation step is applied on the vehicle count features for each site. Min-max is chosen as this ensures the minimum value for vehicle counts will be 0 and standardisation has been shown to improve performance [28]. This standardisation is not done on the other features as they are time-based.

### 5.1.2 ANN Training and Validation

For training, the corresponding LA AADT values per vehicle type [5], shown in Table 3.1.2, are concatenated to each count site dataset. These are the ground truth values to be predicted, and so the model is effectively multi-regression. LA AADT is calculated by taking the individual count site vehicle type AADT's (by direction), and selecting the maximum value. The maximum value is chosen after it was found that the median and mean values produced systematic under-estimations at the emissions part of the pipeline. In addition, in the context of emissions, it is suitable to produce a "worst case" estimation, which the maximum AADT value would represent.

To ensure unbiased evaluation of the performance of the model, the models are trained and validated up to and including 2017, while 2018 is kept as the implementation/test year. This was designed together with the satellite image acquisitions discussed in Section 4.2, ensuring the images were acquired in 2018.

The ANN LA AADT model architecture and hyper-parameters are shown in Appendix J. Each count site has its' own model, trained on that specific count site dataset. This is due to the different patterns of traffic flow at each count site and the large amount of data available (approximately 32,000 data-points per count site). Thus, a separate model for each count site will likely provide the best performance. As an example, the training and validation curves for the Havering count site M25/5790A are shown in Figure 5.1. The other LA's showed similar training and validation curves which can be found in Appendix K.

The validation MAPE's at the end of training are between 0 and 0.2. An early stopping criterion with a patience of 3 was implemented to ensure no overfitting occurs.

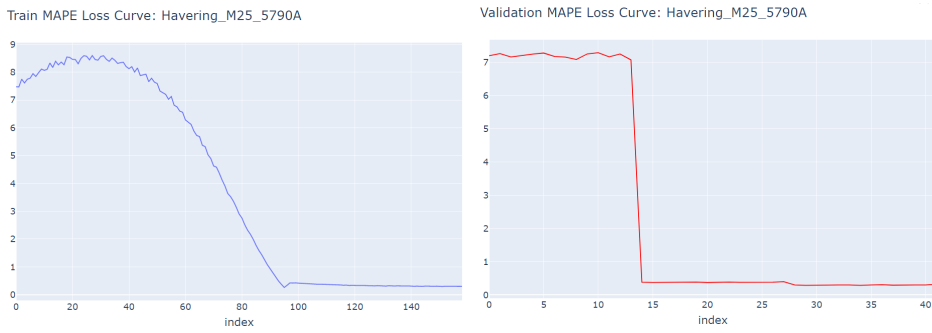


**Figure 5.1:** Havering M25/5790A LA AADT Training and Validation Curves

### 5.1.3 AADT Prediction

To make a prediction of LA AADT from a count site, the following steps are done:

1. Load the model weights for the LA and count site
2. Load traffic count prediction and transform using saved min-max parameters
3. Load historical or estimated speed data (in this evaluation, historical data is used)
4. Load time data (from satellite image) as month, day and hour
5. Concatenate transformed traffic counts, speed and time data and feed into model

Producing an LA AADT for each direction of travel allows for the mean value to be calculated. As some predictions are over-estimates, while others will be under-estimates, this could further improve the accuracy as the mean value will often be closer to the true value. The mean value is used for the metric calculations as it was found to improve results on the majority of count sites chosen.

### 5.1.4 Results

Table 5.1 shows the RMSE and MAPE evaluation metrics on the overall LA AADT results using true speed data. It is difficult to make direct comparisons to state-of-the-art results due to practical differences, such as those discussed in Section 2.3.6.

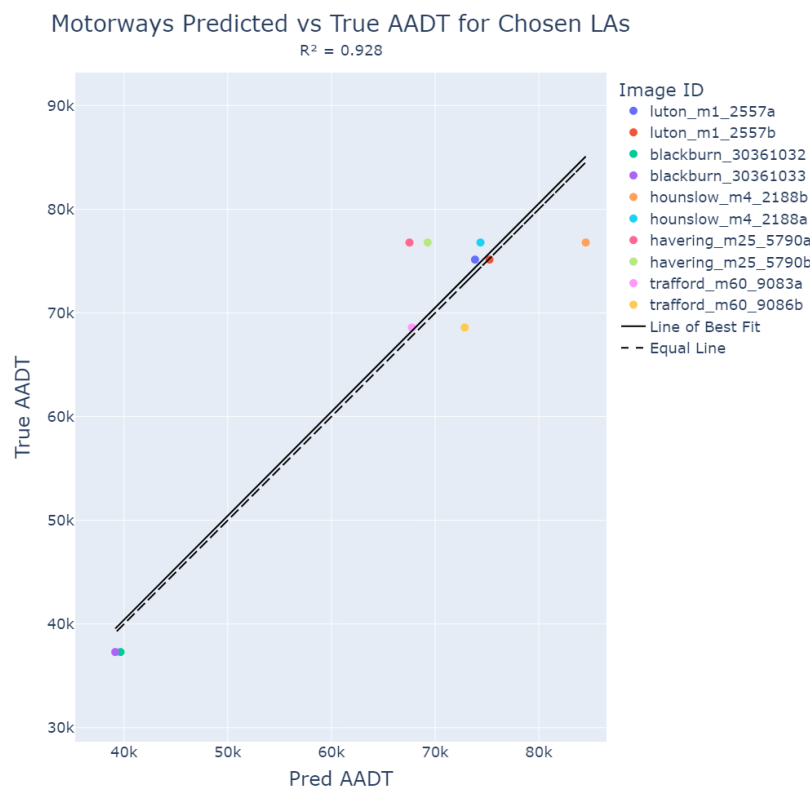
However, Ganji et al. [38] is perhaps the closest study in relation to AADT prediction as they predict AADT across major roads in Toronto, Canada, where they achieve an  $R^2$  value of 0.78. Our results in the base pipeline are limited to motorways, where we achieve an  $R^2$  of 0.92. In addition, the ANN model is able to improve on the higher errors seen for the 15-minute traffic counts by treating it as noise, representing its' robustness. Currently, there are no public studies similar to ours conducted in the UK.

Figure 5.2 shows the predicted vs true overall AADT values for the five chosen LA's, as well as a bar chart showing AADT MAPE values on a per vehicle type basis. Note:

**Table 5.1:** LA AADT Results Table

LA	RMSE	MAPE
Blackburn with Darwen	4433	0.13
Havering	5779	0.087
Luton	703	0.0099
Hounslow	7714	0.15
Trafford	758	0.013
AVERAGE	3878	0.077

The buses and coaches class is removed from the MAPE figure due to significantly worse performance than the other classes, thus distorting the scales. The average MAPE for buses and coaches is 0.8.



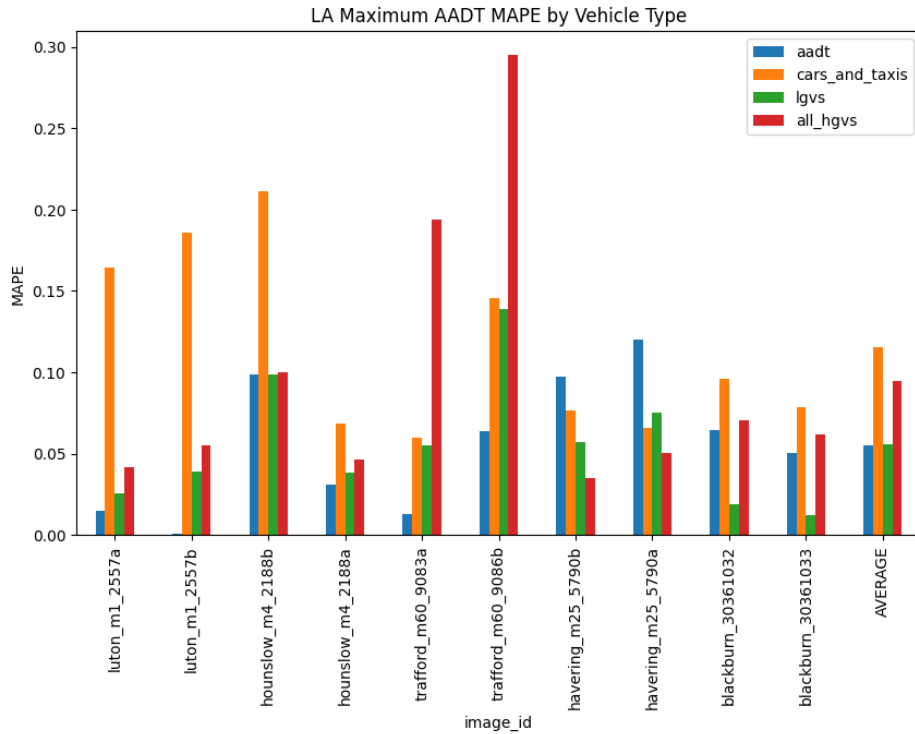


**Figure 5.2:** LA Predicted vs True AADT Scatter plot (top) and AADT MAPE by Vehicle type (bottom)

## 5.2 Motorway LA GHG Emissions

### 5.2.1 Emissions Calculation

Table 5.2 shows the variables and their respective values for calculating GHG emissions. Total length of motorway values are published by the DfT [6], GHG conversion factors are published by DESNZ and BEIS [18] and fuel consumption is published by DfT [19].

The equation for calculating annual GHG emissions per vehicle type,  $i$ , in an LA, using vehicle type data is:

$$\begin{aligned}
 \text{VKT}_i &= \text{AADT}_i * \text{Total Motorway Length} * 365 \\
 \text{Litres}_i &= \text{VKT}_i / \text{Specific Fuel Consumption} \\
 \text{GHG Emissions}_i &= \text{Litres}_i * \text{GHG Conversion Factor}
 \end{aligned} \tag{5.1}$$

The total GHG emissions is then calculated as the sum of emissions across all vehicle types.

We use the 2012 fuel consumption values from the DfT [19]. The relevant fuel types for GHG conversion factors are petrol and diesel, for which we assume the average bio-fuel blend as this is found in normal petrol stations. In addition, the

vehicle licensing dataset [20] shows that in 2017 petrol cars accounted for 59% of all licensed cars, while diesel cars accounted for 40% and electric/hybrid cars were 1%. This weighting is applied to the conversion factors to represent this fuel type distribution.

**Table 5.2:** LA GHG Emissions Variables

GHG Emissions Variable	Value	Source
Total length of motorway in the LA	km	DfT [6]
Luton	4.18	
Blackburn	12.87	
Hounslow	15.77	
Havering	19	
Trafford	9.98	
GHG Conversion factors by fuel type	kg CO <sub>2</sub> e	DESNZ and BEIS [18]
Petrol cars	2.16	
Diesel cars	2.56	
Fuel consumption (2012)	km/litre	DfT [19]
Petrol cars	20	
Diesel cars	23	
Petrol LGV's	18.4	
Diesel LGV's	17.1	
HGV's	3.6	
Vehicle Licensing weighting (2017)	Percentage	DfT [20]
Petrol	59	
Diesel	40	

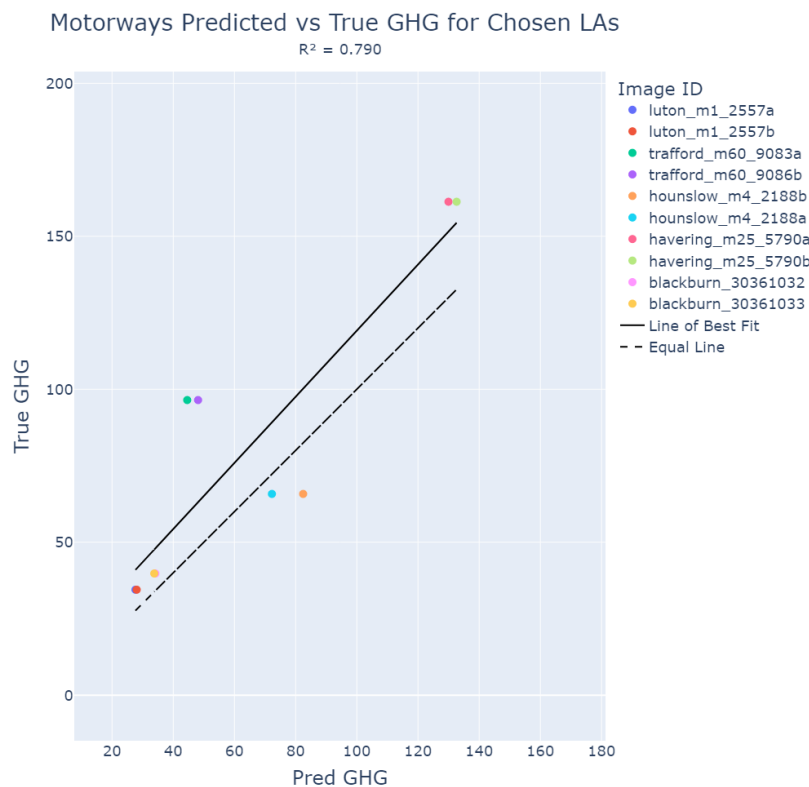
## 5.2.2 Results

Table 5.3 shows the RMSE and MAPE evaluation metrics for annual LA GHG Emissions prediction, where we report an average MAPE of 0.24. Figure 5.3 shows the predicted vs true GHG emissions values for the five chosen LA's. The  $R^2$  coefficient is 0.79, representing a good fit.

For similar reasons to AADT, direct comparisons to other state-of-the-art emissions predictions is difficult. Ganji et al. [38] is perhaps the closest study, where they predict emissions in 2015 for the city of Toronto, Canada to be 6.0823 million tonnes/yr, while the Atmospheric Fund (TAF) for 2015 for Toronto was 5.25 million tonnes/yr (TAF, 2018) [38]. This represents an MAPE of 0.15. Currently, there are no public studies similar to ours conducted in the UK.

**Table 5.3:** LA GHG Results Table

LA	RMSE	MAPE
Blackburn with Darwen	8.32	0.21
Havering	32.8	0.20
Luton	6.61	0.19
Hounslow	6.66	0.10
Trafford	45.7	0.47
AVERAGE	20.0	0.24



**Figure 5.3:** LA Mean Predicted vs True GHG Scatter Plot

### 5.3 Motorway Evaluation

Figure 5.4 displays the predicted and true LA AADT and GHG emissions in a single graph. For predictions, we display the mean value across the two count sites in each LA. Circle markers represent predictions, while star markers represent true values. The results show that the pipeline is able to accurately estimate LA GHG road emissions on motorways using AADT values per vehicle type. The lack of strong positive correlation found during EDA in Section 3 is captured by the pipeline.

However, Trafford seems to be an outlier in its' results as shown by the large er-

ror between emissions ground truth and predicted values. This is in spite of Trafford not exhibiting outlier properties during EDA, as well as Trafford having low LA AADT MAPE. An investigation into Trafford variables used in the pipeline does not reveal any anomalies, thus this could potentially be due to a limitation in the pipeline, or an error in the data.

Another interesting LA is Luton, as this did exhibit outlier properties in data analysis as shown by its high AADT value but low emissions, however the pipeline results agree with the data. Further investigation showed that low emissions is due to small motorway total length, while high AADT is likely due to an airport within the LA.

In terms of model performance on a vehicle type basis, from Figure 5.2 we can see that the model struggled to learn the patterns associated with the buses and coaches vehicle type. This is likely because most data-points contained zero buses and coaches, and thus there was a high class imbalance in this sense. Interestingly, LGV's produce MAPE values similar to overall AADT, while cars and taxis and HGV's have MAPE values as approximately double. This indicates that LGV traffic flow patterns on motorways are less noisy than other vehicle types. A possible limitation of the pipeline is the lack of inclusion of the surrounding area variables to the motorway road segment. For example, the presence of a school, university or business park coming off the motorway could be an important variable for cars and taxis, hence its' omission could be a reason for the higher cars and taxis' MAPE.

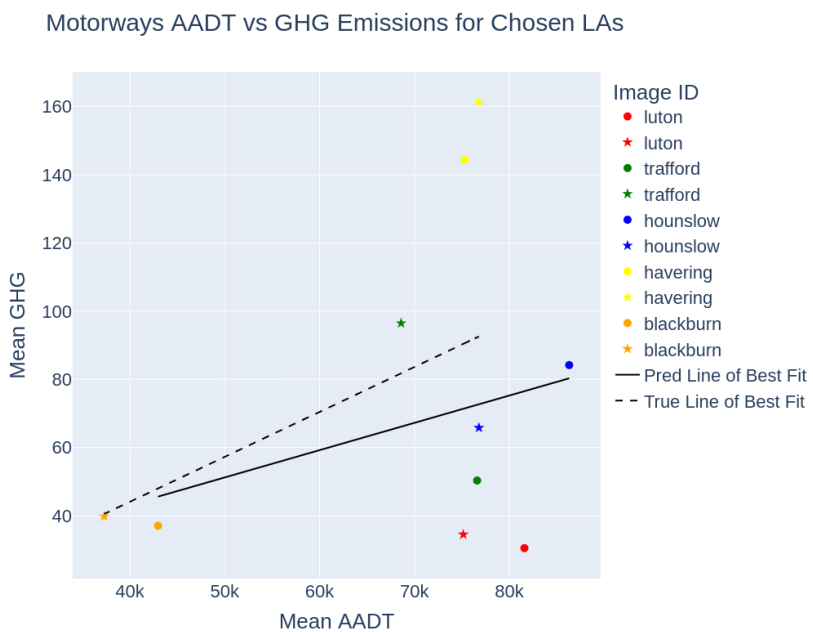


**Figure 5.4: LA AADT and GHG Scatter Plot**

### 5.3.1 Implementation without Vehicle Type Data

Predicting LA AADT on a vehicle type basis is used as this improves results compared to using a single AADT value. However, in relation to the UN SGD goals on Climate

Action and Sustainable Cities and Communities, an alternative method is developed to calculate GHG emissions from a single AADT value, for use in regions where data on AADT per vehicle type is not available. The method uses the satellite image to estimate the distribution of vehicle types using object classification, and is as follows:

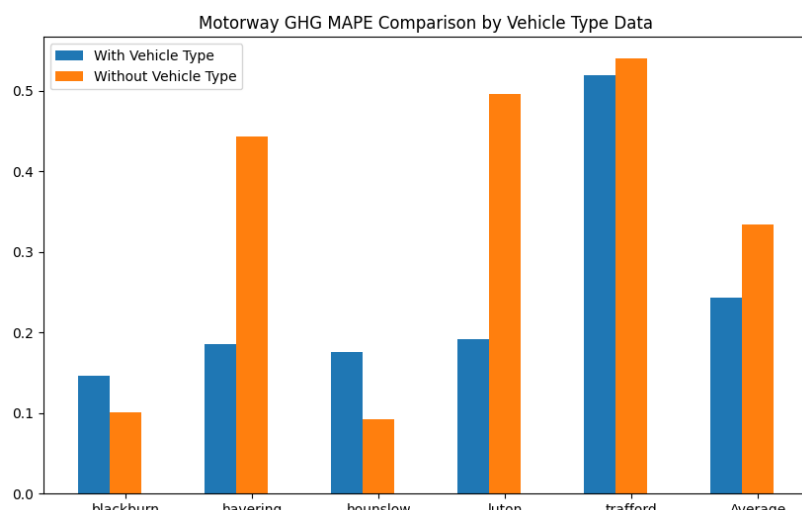
1. Vehicle type mapping: Load vehicle object detection results and convert the vehicle type classes from the xView dataset into valid categories from the UK dataset
2. AADT assignment: Assign predicted overall AADT proportionally to each detected vehicle type

Table 5.4 shows the specific mappings for each xView vehicle class to the UK class.

**Table 5.4:** Vehicle Type Class Mappings Table

xView Class	UK Dataset Class
Passenger vehicle, Small car, Passenger car	Cars and Taxis
Pickup Truck, Utility Truck, Truck, Trailer, Truck w/ Box, Trailer, Cargo car	LGV's
Cargo Truck, Truck Tractor, Truck w/ Flatbed, Truck w/Liquid	HGV's
Bus	Buses and coaches

The rest of the GHG emissions calculation is the same as with vehicle type data. Figure 5.5 shows the bar plot comparison of with and without vehicle type data for motorways. The no vehicle type scatter plot of AADT vs GHG emissions can be found in Appendix L, where circle markers represent predictions and star markers represent true values.



**Figure 5.5:** MAPE Comparison for emissions calculations without Vehicle Type Data

As expected, not using AADT on a vehicle type basis reduces the accuracy in the emissions calculations, with the average MAPE reducing by around 0.1. Trafford remains as an outlier in its' MAPE, while Luton and Havering both see increases of 0.2 and 0.3 MAPE respectively for without vehicle type data.

Interestingly, Blackburn and Hounslow see decreases in MAPE for without vehicle type data. This is likely because in the satellite image, the object detection model has detected more LGV's and HGV's than is represented in the yearly AADT distributions. As LGV's and HGV's have higher fuel consumption, the GHG emissions prediction will be higher.

Overall, using AADT vehicle type data is a way of introducing robustness to the noise of using a single satellite image to estimate vehicle type distributions.

## 5.4 Parametric Analysis

In this section, we analyse the effect of changing parameter values on results, primarily measured using the MAPE metric for its scale independence. The parametric analysis conducted in this section is not exhaustive and does not consider all potential values. A parameter is omitted from analysis if either a) its' distribution variance is minimal or 0 or b) it would require significant re-configurations to the pipeline.

We present the average MAPE results with and without the Trafford LA. This is due to the Trafford result discussed in Section 5.3 showing an MAPE of 2 times higher than other LAs. Thus, it is possible that it is an outlier and this should be taken into account during parametric analysis.

### 5.4.1 LA AADT Statistics

To train the ANN LA AADT model, a statistical value of the LA AADT's are required as the target variable. The maximum value was used for achieving the best results. For this parameter, we investigate the effect of using different statistics on results.

Central tendency statistics were the initial focus, however proved to systematically underestimate GHG emissions. Figure 5.6 shows the mean, median and maximum value MAPE bar charts for AADT and GHG emissions estimation. It can be seen that AADT and GHG emissions MAPE errors differ only slightly for maximum and mean values, whereas the median has noticeably worse performance. In addition, the statistics behave similarly with and without including Trafford.

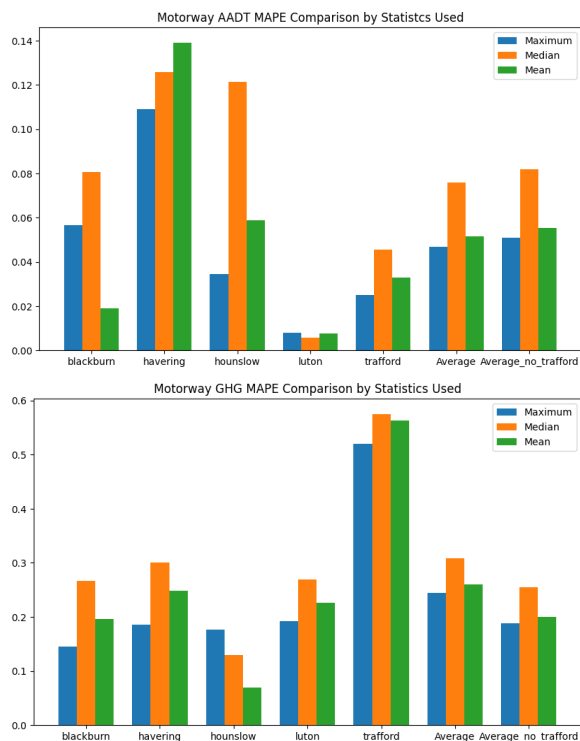


**Figure 5.6:** MAPE Comparison of Different Statistics for LA AADT

A likely reason for this behaviour is as a result of the bias towards underestimation of 15-minute traffic counts due to the object detection model missing vehicles (false negatives). This effect of this bias is reduced when using the mean or maximum as they tend to result in higher values than the median, thus AADT and GHG emissions prediction benefits from this on average.

#### 5.4.2 Traffic Counts and Speed

Inputs into the ANN for LA AADT prediction include traffic counts, average speed and time. The effect of traffic counts and speed on AADT and GHG emissions prediction is analysed in this section. For true speed data at satellite image acquisition times, see Table 4.3.

Figure 5.7 shows the MAPE effect of increasing and decreasing the traffic count and speed values by 50% independently on GHG Emissions. For the effect on AADT, see Appendix M.

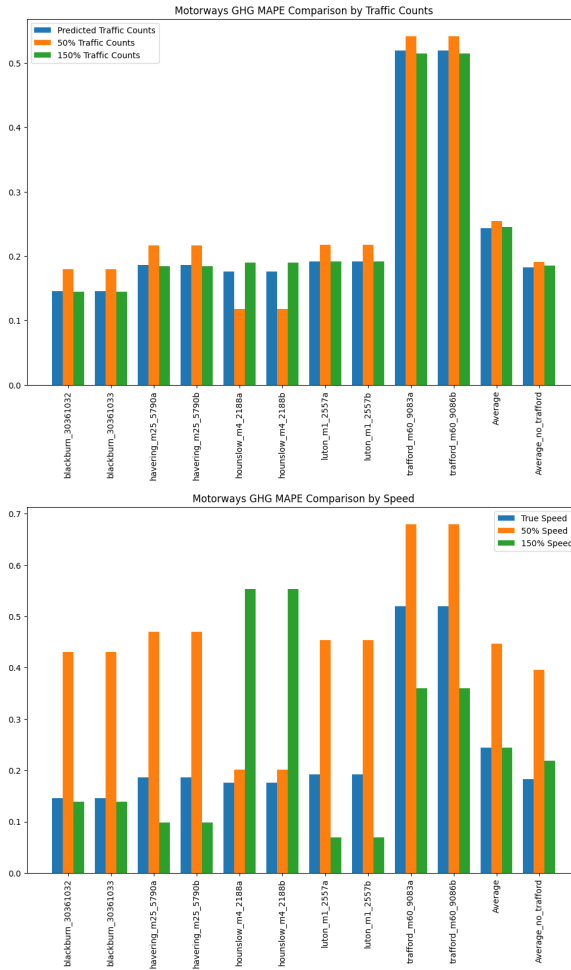


Figure 5.7: Effect of Traffic Counts and Speed on GHG Emissions MAPE

It is shown that traffic count vehicle volumes do not affect GHG emissions estimation. This is likely due to the ANN, trained on historical traffic counts, learning that vehicle volumes have high levels of noise and thus do not impact the AADT predictions because the model has learnt to ignore noise. This can be seen in Appendix M. Trafford remains an outlier in MAPE for all traffic count values.

On the other hand, average speed plays an important role for AADT and emissions estimation, as shown by the significant change in MAPE between true speeds and 50% speeds. However, interestingly, true speed and 150% speed GHG emissions MAPE are almost equal on average. This suggests non-linearity in the speed parameter on emissions in this pipeline. Looking at specific LAs, Hounslow is the only one that experiences an increase in MAPE for 150% speed values, and it experiences minimal change for 50% speeds. Excluding Trafford has a minimal effect on average MAPE.

### 5.4.3 GHG Emissions Variables

Fuel consumption and GHG conversion factors both rely on parameters to define a distribution. For example, fuel consumption for heavy goods vehicle depends heavily on whether it is full or not, while conversion factors depend on the grade of fuel. We omit GHG conversion factors from parameteric analysis due to its' minimal distribution variance from the DfT [18].

In this section, we analyse the effect of the fuel consumption parameter on predicting emissions by varying the values by 50% for each vehicle type. Figure 5.8 shows the LA Motorway GHG Emissions MAPE by fuel consumption parameter for comparison. The higher and lower values represent a 50% increase and decrease in fuel consumption respectively, from the base case of 2012 fuel consumption values that are used in the main pipeline.

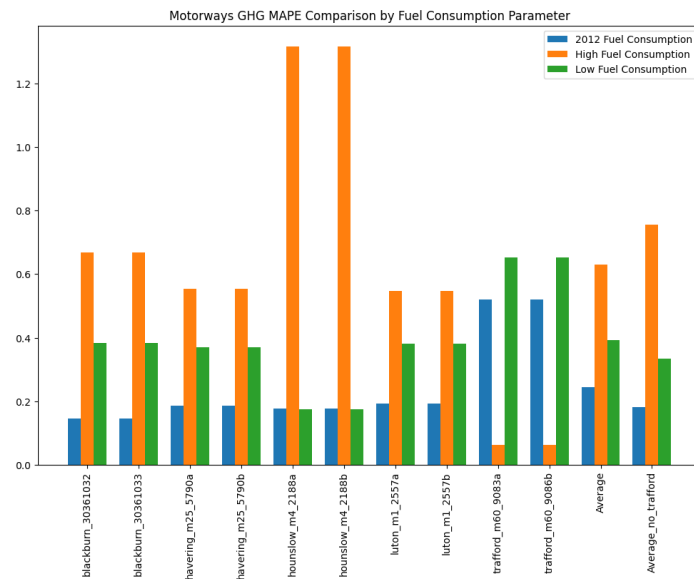


**Figure 5.8:** LA Motorway GHG Emissions MAPE by Fuel Consumption Parameter

We can see a greater degree of sensitivity to the higher value than lower, suggesting non-linearity in the effect of the fuel consumption parameter to GHG emissions. The Trafford LA also shows significantly lower MAPE for the higher value, showing that the main pipeline underestimates emissions there as an outlier. The Hounslow LA shows the opposite effect, whereby a high fuel consumption leads to significantly higher MAPE values than the lower fuel consumption. This indicates that fuel consumption values impact each LA differently, possibly due to the wide difference's in motorway total lengths within each LA. Including or excluding Trafford does not significantly impact the average MAPE.

## 5.5 Extension to Other Road Types

While the satellite images and 15-minute traffic counts data comes from motorway sections, the methods used for LA AADT and emissions calculations can be extended

to other road types.

Here, the ANN for LA AADT prediction uses the LA AADT value for A-Roads and Minor Roads respectively as the target variable. Thus, it is trained to learn transformations from motorway traffic data to nearby road traffic (i.e. within the same LA). Appendix N shows the ANN training and validation curves for the same chosen count sites.

The following points summarise the required value changes when doing AADT and GHG emissions prediction on other road types. The dataset sources used for motorways are the same as for A-roads and minor roads and can be filtered as appropriate.

- ANN LA AADT prediction target variable and ground truth
- Emissions variables (total road length and km/litre )
- Emissions ground truth data

### 5.5.1 A-Roads Results

This section investigates the LA AADT and GHG emissions results for A-Roads. Minor roads were also investigated, however produced significantly higher errors than A-Roads and motorways. Appendix P shows the results for minor roads.

Tables 5.5 and 5.6 show the mean MAPE results for A-Roads AADT and MAPE for each LA. The average MAPE values of 0.1 and 0.2 respectively show it is likely that motorway traffic counts are a good predictor of A-road traffic flow and GHG emissions. Appendix O show the scatter plots of AADT and GHG emissions respectively.

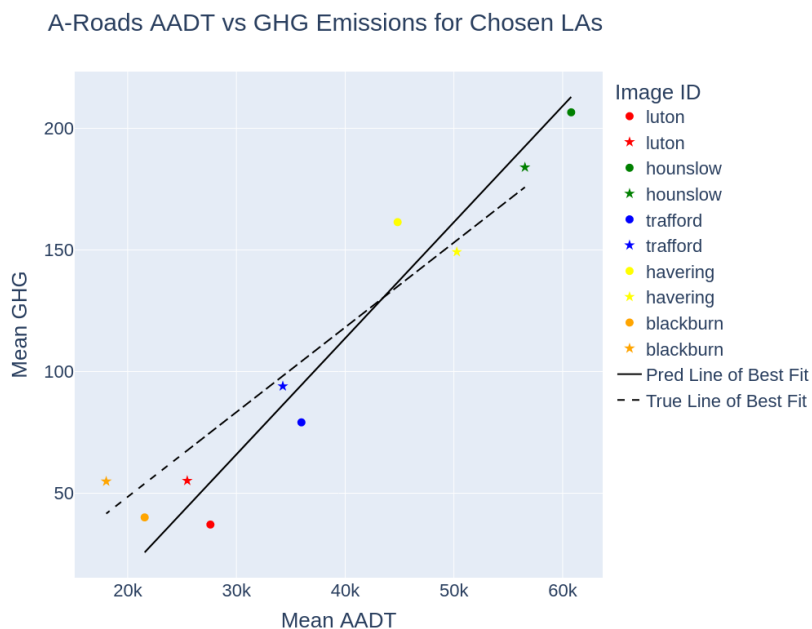
**Table 5.5:** A-Roads LA AADT Results Table

LA	RMSE	MAPE
Blackburn with Darwen	3533	0.20
Havering	5442	0.11
Luton	2131	0.08
Hounslow	4253	0.07
Trafford	1710	0.05
AVERAGE	3414.0	0.10

Figure 5.9 shows a scatter plot of the predicted and true AADT vs GHG Emissions. Circle markers represent predictions, while star markers represent true values. Overall, the results show that the pipeline developed for satellite images of motorways can be successfully extended to A-roads with minimal changes shown by the similar results.

**Table 5.6:** A-Roads LA GHG Results Table

LA	RMSE	MAPE
Blackburn with Darwen	14.7	0.27
Havering	32.8	0.08
Luton	18.0	0.33
Hounslow	22.6	0.12
Trafford	14.9	0.16
AVERAGE	16.5	0.19


**Figure 5.9:** LA A-Roads AADT vs GHG Emissions Scatter Plot

### 5.5.2 Evaluation

Comparisons between motorways, A-Roads and minor roads results are investigated and discussed in this section. Given that the satellite images, 15-minute traffic counts and LA AADT AAN training derives from motorways, it is expected that motorway performance of the pipeline should be the best, especially when evaluating AADT results.

A-Roads are the most similar traffic data distribution to motorways, as concluded in Section 3. Thus, we expect A-road performance to be similar to motorway performance, but slightly worse due to the high level of spatial correlation found.

Minor roads vary considerably in traffic data distribution and road characteristics, for example with speed limits. This variability makes AADT predictions and emissions calculations less accurate. Thus, minor road performance should be the worst

of the 3 road types investigated.

Figure 5.10 shows the MAPE comparisons for AADT and GHG emissions by road type as bar plots.

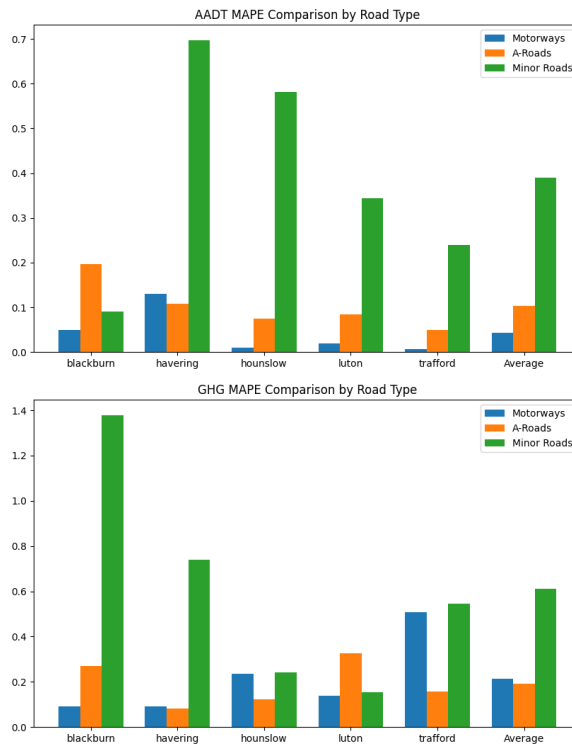


**Figure 5.10: LA AADT and GHG MAPE By Road Type Comparison**

As expected, motorways and A-Roads have comparable MAPE performance across AADT and GHG emissions, while minor roads show considerably higher MAPE values. The ANN is able to better predict LA AADT from motorways as it is trained on motorway traffic count data. Interestingly, Trafford is not an outlier in its MAPE for A-roads as it is for motorways. In addition, A-Roads exhibit a higher positive correlation between AADT and GHG emissions than motorways. This can be seen by comparing Figures 5.9 and 5.4.

# **Chapter 6**

## **Ethical issues**

Using satellite imagery comes with a wide range of ethical issues to consider. However, for this projects' use case, the most relevant consideration would be if the satellite image results were able to identify someone/a group of people.

The most obvious example would be through the unintended ability to be able to read license plates from vehicles in the image. This is an ethical issue as the people in the image have not consented to their license plate being readable. However, this issue is mitigated because the model is only able to detect vehicles and classify them, not read license plates. In addition, it is unlikely that satellite images used will be of high enough spatial resolution to read license plates.

Apart from the satellite images, all datasets and models used are publicly available and free, thus mitigating the ethical issues with using them.

# Chapter 7

## Conclusions and Future Work

### 7.1 Conclusion

In conclusion, we present a pipeline that consists of two main parts. The input into the pipeline is a raw satellite image that contains a motorway section. The first part of the pipeline takes the raw satellite image and produces traffic count predictions of count sites from the motorway section within the image. The second part of the pipeline takes the predicted traffic counts and produces estimates of Average Annual Daily Traffic (AADT) and Greenhouse Gas (GHG) emissions at the Local Authority (LA) level. The full pipeline is shown in Figure 2.3.

Due to the practical nature of the project, many stages of the pipeline have assumptions and/or requirements. Table 7.1 summarises each requirement, the criteria, its' reasoning and the source, for the full pipeline. Where pipeline extensions negate a previous assumption or requirement, they are omitted. An example is discussed in Section 5.3.1, which negates the requirement for vehicle type data.

This project therefore builds upon previous research in various areas around road transportation, speed estimation and emissions prediction from satellite imagery. To that end, it produces an end-to-end pipeline with novel contributions and insights with the overall aim of providing a way to monitor progress towards the UN Sustainable Development Goals (SGD's), specifically those centred around Climate Action and Sustainable Cities and Communities.

#### 7.1.1 Motorway Traffic Counts

Traffic count prediction from satellite imagery has been investigated by Kaack et al. [33], Ganji et al. [28] and Jake Baker [26]. However, this part of the pipeline introduces the flexibility of using live speed estimation, by taking advantage of the time lag between MS bands of WV-2/3 satellites, inspired by the paper from Salehi et al. [3].

We demonstrate that reasonable traffic count results are possible using speed estimation, as MAPE performance reduced 0.2 on average. While this may not be

**Table 7.1:** Pipeline Requirements Table

Requirement	Criteria	Reasoning	Source
Satellite image acquisition date and time	Month, Day, Hour	Required for LA AADT prediction	ESA [41]
Satellite image has minimal cloud cover	$\leq 5\%$ cloud cover	Acceptable object detection model performance	ESA [41]
Historical 15-minute traffic count data with average speeds	$\leq 10\%$ missing values	LA AADT Training (input variables)	DfT [4]
Road network shapefile	All road cover within the LA and updated at the inference year	Automated QGIS Pre-processing (otherwise manual clipping required)	DfT [5]
LA AADT	At least one count site within the LA	LA AADT Training (target variable)	DfT [5]
Total road length	Updated at the inference year and covers all road length within LA	LA emissions calculation	DfT [6]
4 vehicle types	HGV's, LGV's, Buses and Coaches, Cars and Taxis	UK LA AADT dataset compatibility	DfT [5]
Fuel consumption data	Values for each vehicle type	LA emissions calculations	DfT [19]
Road vehicle licensing statistics	Petrol, diesel, hybrid and electric vehicle types	LA emissions calculation	DfT [20]

required in regions like the UK, where motorway speed data is readily available, this will likely prove useful in regions where data is not available.

### 7.1.2 LA AADT

Recent developments in AADT prediction involve using Artificial Neural Network's (ANN's) to learn transformations between traffic counts and AADT, which have been seen to outperform traditional methods.

Therefore, this pipeline introduces ANN training, validation and implementation for predicting motorway LA AADT [5] using just motorway traffic counts from a single count site. All necessary inputs for ANN training and implementation can be extracted from the satellite image, for example speed estimation and time of day. We use 2017 as the train year and 2018 as the test year and show state-of-the-art results, achieving an MAPE of less than 0.1 and  $R^2$  score of greater than 0.9.

In addition, the pipeline introduces the novel ability to predict motorway LA AADT on a per vehicle type basis with the following vehicle types: cars and taxis, buses and coaches, Light Goods Vehicles (LGV's) and Heavy Goods Vehicles (HGV's). This is important when estimating annual GHG emissions.

Ganji et al. [28] goes further by predicting AADT on nearby roads using regression methods. Our solution was instead to train separate ANN's to learn the transformations from motorway traffic data to other road types, in the same LA. For A-roads, this produced similar error results to motorway predictions, within 0.05 MAPE. However, for minor roads, performance was significantly lower, by around a factor of 5.

Finally, an investigation into the effect of using different LA AADT statistics and ANN input values was conducted. For LA AADT, it was found that using the maximum value produced best results, likely due to the YOLOv5 object detection model having a bias towards under-estimation of vehicle counts. For ANN input values, we found that varying traffic volumes had minimal impact on results, whereas speed had a non-linear and significant impact on results.

### 7.1.3 LA GHG Emissions

Calculating GHG emissions is done using UK data on fuel consumption [19], GHG conversion factors [18], road length statistics [6] and vehicle licensing statistics [20]. By applying this on the vehicle type basis and scaling the values to the LA level, we are able to estimate the emissions from each vehicle type. Summing them together produces the total annual GHG emissions from road transport on motorways.

The pipeline introduces a novel method of estimating emissions when data on AADT per vehicle type is not available. We use the object classes detected from the ob-

ject detection model to estimate the distribution of vehicle types by mapping xView classes to UK dataset classes for compatibility. We show that this produces results that are slightly worse, within 0.1 MAPE, than when using vehicle type data.

Estimating GHG emissions on different road types in the same LA was also investigated, using their respective predicted LA AADT values. We found that A-roads produced similar error results to motorway estimations, within 0.05 average MAPE. However, minor roads emissions estimation showed significant performance degradation.

Finally, we perform parametric analysis on emissions performance by increasing and decreasing pipeline variables. Notable findings are that traffic counts are not as impactful as speed or fuel consumption for emissions prediction, and that the maximum AADT value produces the best results as a parameter for LA AADT.

## 7.2 Future Work

There are several paradigms for which immediate improvements can be made on this study and project pipeline. Future work should be prioritised to the developments for the project goals, which primarily come from monitoring progress towards the UN SGD's of Climate Action and Sustainable Cities and Communities. To that end, many would stem from reducing the requirements outlined in Table 7.1.

In addition, the results from the parametric analysis in Section 5.4 gives a good indication of which parts of the pipeline are most important to emissions MAPE. Thus, we list these parts in descending order of impact as a suggestion to where future work should be prioritised:

1. Fuel Consumption: the distribution of values has a high variance and Figure 5.8 shows this can have a significant impact. In addition, in this study we assume the same fuel consumption parameters for motorways, A-Roads and minor roads, when in reality they differ. For example, motorways often have the lowest fuel consumption.
2. Average Speed: We demonstrate the extension of Salehi et al. [3] to better suit the project goals, however as shown in Figure 5.7 it is worth optimising this further due to its' impact on emissions prediction.
3. LA AADT Statistics: This parameter influences the target variable of ANN prediction which in turn affects emissions prediction, however from Figure 5.6 we can see that the MAPE differences are not as wide as for speed and fuel consumption
4. Traffic Counts: traffic counts (number of vehicles passing through a count site in 15-minutes) proved to not be a significant indicator of LA AADT prediction in this study, as shown in Figure 5.7

A limitation of this list is that it is not exhaustive as not all model parameters were analysed. In the rest of this section, we list a couple examples of future works based off the research done in Section 2.

Currently, the pipeline depends on QGIS pre-processing. Section 2.3 discusses the rising performance of DL models for road segmentation, which could be introduced into the satellite pre-processing stage to replace the QGIS based method. Some benefits of this would be improved scalability in imagery pre-processing through automation, as well as no longer relying on road network geographical data.

Introducing more classes into the LA AADT and emissions calculation would provide more accuracy to the estimations. For example, the pipeline currently averages all HGV's into a single class. However, separating these into, for example, Rigid and Arctic HGV's would likely boost accuracy. In addition, as the train year is 2017 and test year is 2018, DfT data [20] shows that only 2% of cars were electric. The rapid rise of electric and hybrid cars for predicting emissions in more recent and future years would benefit from being more explicitly accounted for in the pipeline, for example by including a charging emissions parameter.

# Bibliography

- [1] Biermann F, Kanie N, Kim RE. Global governance by goal-setting: the novel approach of the UN Sustainable Development Goals. *Current Opinion in Environmental Sustainability*. 2017;26:26-31. pages 2
- [2] Lamb WF, Wiedmann T, Pongratz J, Andrew R, Crippa M, Olivier JG, et al. A review of trends and drivers of greenhouse gas emissions by sector from 1990 to 2018. *Environmental research letters*. 2021;16(7):073005. pages 2
- [3] Salehi B, Zhang Y, Zhong M. Automatic Moving Vehicles Information Extraction From Single-Pass WorldView-2 Imagery. *IEEE Journal of Selected Topics in Applied Earth Observations and Remote Sensing*. 2012;5(1):135-45. pages 3, 11, 15, 26, 32, 35, 54, 57
- [4] Highways England. Traffic Flow Data; Published: N/A. Accessed: April 6, 2023. URL: <https://tris.highwaysengland.co.uk/detail/trafficflowdata>. pages 4, 14, 15, 16, 31, 37, 55
- [5] Department for Transport. Local Authorities Road Traffic Data; Published: N/A. Accessed: April 6, 2023. URL: <https://roadtraffic.dft.gov.uk/>. pages 4, 14, 17, 18, 38, 55, 56
- [6] Department for Transport. Road Length Statistics (RDL); 2023. Accessed: May 16, 2023. URL: <https://www.gov.uk/government/statistical-data-sets/road-length-statistics-rdl>. pages 4, 14, 41, 42, 55, 56
- [7] Drouyer S. Vehsat: A large-scale dataset for vehicle detection in satellite images. In: IGARSS 2020-2020 IEEE International Geoscience and Remote Sensing Symposium. IEEE; 2020. p. 268-71. pages 5, 14
- [8] Haroon M, Shahzad M, Fraz MM. Multisized object detection using spaceborne optical imagery. *IEEE Journal of Selected Topics in Applied Earth Observations and Remote Sensing*. 2020;13:3032-46. pages 5
- [9] Xia GS, Bai X, Ding J, Zhu Z, Belongie S, Luo J, et al. DOTA: A large-scale dataset for object detection in aerial images. In: Proceedings of the IEEE conference on computer vision and pattern recognition; 2018. p. 3974-83. pages 5, 10

- [10] Lam D, Kuzma R, McGee K, Dooley S, Laielli M, Klaric M, et al. xvview: Objects in context in overhead imagery. arXiv preprint arXiv:180207856. 2018. pages 5, 14, 29
- [11] Mundhenk TN, Konjevod G, Sakla WA, Boakye K. A large contextual dataset for classification, detection and counting of cars with deep learning. In: European conference on computer vision. Springer; 2016. p. 785-800. pages 5
- [12] Razakarivony S, Jurie F. Vehicle detection in aerial imagery: A small target detection benchmark. Journal of Visual Communication and Image Representation. 2016;34:187-203. pages 5
- [13] Lin HY, Tu KC, Li CY. Vaid: An aerial image dataset for vehicle detection and classification. IEEE Access. 2020;8:212209-19. pages 5
- [14] Wang J, Teng X, Li Z, Yu Q, Bian Y, Wei J. VSAI: A Multi-View Dataset for Vehicle Detection in Complex Scenarios Using Aerial Images. Drones. 2022;6(7):161. pages 5
- [15] Department for Transport. Transport and Environment Statistics 2021 Annual report; Published: 2022. [https://assets.publishing.service.gov.uk/government/uploads/system/uploads/attachment\\_data/file/984685/transport-and-environment-statistics-2021.pdf](https://assets.publishing.service.gov.uk/government/uploads/system/uploads/attachment_data/file/984685/transport-and-environment-statistics-2021.pdf). pages 5
- [16] Department for Energy Security and Net Zero and Department for Business, Energy Industrial Strategy. UK local authority and regional greenhouse gas emissions national statistics; Published: N/A. Accessed: April 6, 2023. URL: <https://www.data.gov.uk/dataset/723c243d-2f1a-4d27-8b61-cdb93e5b10ff/uk-local-authority-and-regional-greenhouse-gas-emissions>. pages 5, 14, 21
- [17] National Atmospheric Emissions Inventory. Emission factors for transport; Published: N/A. Accessed: May 17, 2023. URL: <https://naei.beis.gov.uk/data/ef-transport>. pages 6
- [18] Department for Energy Security and Net Zero and Department for Business, Energy Industrial Strategy. Greenhouse gas reporting: conversion factors 2022; Published: N/A. Accessed: May 23rd, 2023. URL: <https://www.gov.uk/government/publications/greenhouse-gas-reporting-conversion-factors-2022>. pages 6, 14, 41, 42, 49, 56
- [19] Department for Transport. Energy and environment: data tables (ENV); Published: N/A. Accessed: May 23rd, 2023. URL: <https://www.gov.uk/government/statistical-data-sets/energy-and-environment-data-tables-env>. pages 6, 14, 41, 42, 55, 56

- [20] Department for Transport. Vehicle licensing statistics 2017; Published: N/A. Accessed: May 23rd, 2023. URL: [https://assets.publishing.service.gov.uk/government/uploads/system/uploads/attachment\\_data/file/716075/vehicle-licensing-statistics-2017-revised.pdf](https://assets.publishing.service.gov.uk/government/uploads/system/uploads/attachment_data/file/716075/vehicle-licensing-statistics-2017-revised.pdf). pages 6, 14, 42, 55, 56, 58
- [21] Sharma B, Kumar S, Tiwari P, Yadav P, Nezhurina MI. ANN based short-term traffic flow forecasting in undivided two lane highway. *Journal of Big Data*. 2018;5(1):1-16. pages vi, 6
- [22] Ren S, He K, Girshick R, Sun J. Faster r-cnn: Towards real-time object detection with region proposal networks. *Advances in neural information processing systems*. 2015;28. pages 7
- [23] Terven J, Cordova-Esparza D. A Comprehensive Review of YOLO: From YOLOv1 to YOLOv8 and Beyond. *arXiv preprint arXiv:230400501*. 2023. pages 7
- [24] Lin TY, Goyal P, Girshick R, He K, Dollár P. Focal loss for dense object detection. In: *Proceedings of the IEEE international conference on computer vision*; 2017. p. 2980-8. pages 7
- [25] Padilla R, Netto S, da Silva E. A Survey on Performance Metrics for Object-Detection Algorithms; 2020. . pages vi, 8
- [26] Baker J. Detecting and Modelling Traffic with Satellite Images. To be Submitted. 2022. pages 9, 15, 28, 54
- [27] Li H, Jing L, Tang Y. Assessment of pansharpening methods applied to WorldView-2 imagery fusion. *Sensors*. 2017;17(1):89. pages 9
- [28] Ganji A, Zhang M, Hatzopoulou M. Traffic volume prediction using aerial imagery and sparse data from road counts. *Transportation Research Part C: Emerging Technologies*. 2022;141:103739. pages 9, 10, 11, 15, 38, 54, 56
- [29] Xia Z, Zang Y, Wang C, Li J. Road width measurement from remote sensing images. In: *2017 IEEE International Geoscience and Remote Sensing Symposium (IGARSS)*. IEEE; 2017. p. 902-5. pages 9
- [30] Zhu Q, Zhang Y, Wang L, Zhong Y, Guan Q, Lu X, et al. A global context-aware and batch-independent network for road extraction from VHR satellite imagery. *ISPRS Journal of Photogrammetry and Remote Sensing*. 2021;175:353-65. pages 9
- [31] Chen LC, Papandreou G, Schroff F, Adam H. Rethinking Atrous Convolution for Semantic Image Segmentation; 2017. pages 9
- [32] Maity M, Banerjee S, Sinha Chaudhuri S. Faster R-CNN and YOLO based Vehicle detection: A Survey. In: *2021 5th International Conference on Computing Methodologies and Communication (ICCMC)*; 2021. p. 1442-7. pages 10

- [33] Kaack LH, Chen GH, Morgan MG. Truck Traffic Monitoring with Satellite Images. In: Proceedings of the 2nd ACM SIGCAS Conference on Computing and Sustainable Societies. COMPASS '19. New York, NY, USA: Association for Computing Machinery; 2019. p. 155–164. Available from: <https://doi.org/10.1145/3314344.3332480>. pages 10, 11, 15, 34, 54
- [34] Gong H, Mu T, Li Q, Dai H, Li C, He Z, et al. Swin-Transformer-Enabled YOLOv5 with Attention Mechanism for Small Object Detection on Satellite Images. *Remote Sensing*. 2022;14(12):2861. pages 10
- [35] Akyon FC, Altinuc SO, Temizel A. Slicing Aided Hyper Inference and Fine-tuning for Small Object Detection. 2022 IEEE International Conference on Image Processing (ICIP). 2022:966-70. pages 10, 15, 29, 30, 35
- [36] Blattner M, Mommert M, Borth D. Commercial Vehicle Traffic Detection from Satellite Imagery with Deep Learning. In: ICML 2021 Workshop on Tackling Climate Change with Machine Learning; 2021. . pages 11
- [37] Dorogush AV, Ershov V, Gulin A. CatBoost: gradient boosting with categorical features support. arXiv preprint arXiv:181011363. 2018. pages 11
- [38] Ganji A, Shekarrizfard M, Harpalani A, Coleman J, Hatzopoulou M. Methodology for spatio-temporal predictions of traffic counts across an urban road network and generation of an on-road greenhouse gas emission inventory. *Computer-Aided Civil and Infrastructure Engineering*. 2020;35(10):1063-84. pages 11, 39, 42
- [39] Department for Transport. Road Traffic Estimates, Annual Methodology Note; Published: 2022. URL: <https://www.gov.uk/guidance/road-traffic-statistics-information>. pages 12
- [40] UK Department for Business, Energy Industrial Strategy. Methodology for the UK's Road Transport Emissions Inventory; Published: 2019. URL: [https://uk-air.defra.gov.uk/assets/documents/reports/cat07/1804121004\\_Road\\_transport\\_emissions\\_methodology\\_report\\_2018\\_v1.1.pdf](https://uk-air.defra.gov.uk/assets/documents/reports/cat07/1804121004_Road_transport_emissions_methodology_report_2018_v1.1.pdf). pages 12
- [41] European Space Imaging. European Space Imaging Library; Published: N/A. Accessed: 16/04/2023. URL: <https://www.euspaceimaging.com/image-library/>. pages 20, 55
- [42] Jocher G. YOLOv5 by Ultralytics; 2020. <https://github.com/ultralytics/yolov5>. pages 29

# Appendix A

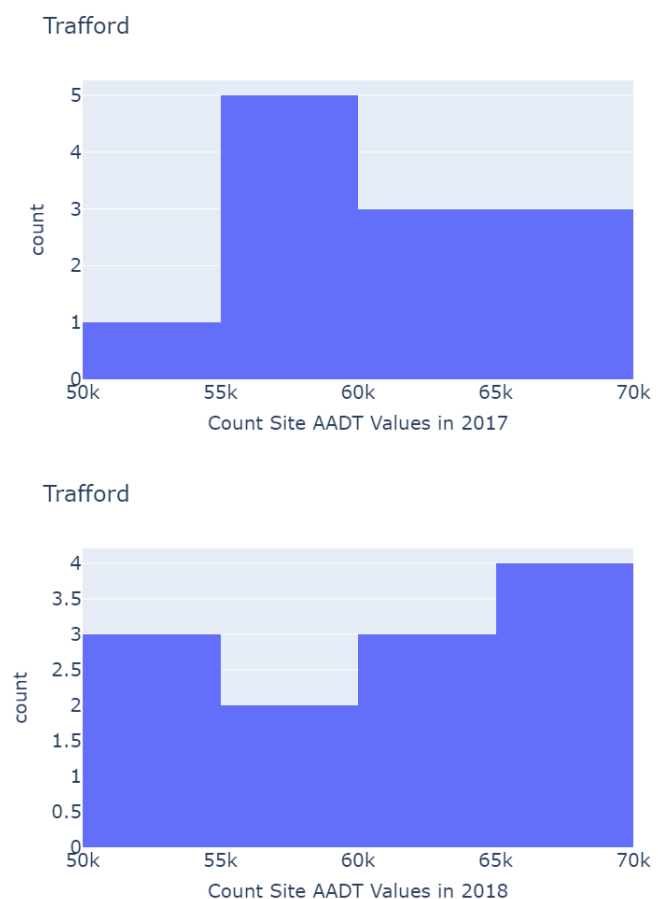
## Satellite Imagery Datasets Summary

Satellite Imagery Datasets Summary	
Dataset	Key characteristics
VEHicle detection in SATellite images (VehSat)	<ul style="list-style-type: none"><li>• Satellite (SkySat, Pleiades, World-View 2 and World-View 3)</li><li>• Published in 2020</li><li>• 8 different areas (e.g. China, USA, Sudan)</li><li>• Single-class (road vehicle)</li><li>• ~4,500 images</li></ul>
Satellite Imagery Multi-vehicles Dataset (SIMD)	<ul style="list-style-type: none"><li>• Satellite (Google Earth)</li><li>• 15 classes (all vehicle)</li><li>• USA and EU regions</li><li>• ~5,000 images</li></ul>
The Dataset of Object deTection (DOTA)	<ul style="list-style-type: none"><li>• 18 classes (wide variety, not only vehicles)</li><li>• Aerial and satellite</li><li>• ~11,000 images</li></ul>
xView	<ul style="list-style-type: none"><li>• WorldView-3 satellite</li><li>• ~60 classes (wide variety, not only vehicles)</li><li>• Large-scale</li></ul>
Non-satellite aerial datasets which contain road vehicle classes:	
<ul style="list-style-type: none"><li>• Cars Overhead With Context (COWC)</li><li>• Vehicle Detection in Aerial Imagery (VEDAI)</li><li>• Aerial Image Dataset for Vehicle detection (VAID)</li><li>- Vehicle detection in complex Scenarios Using Aerial Images (VSAI)</li></ul>	

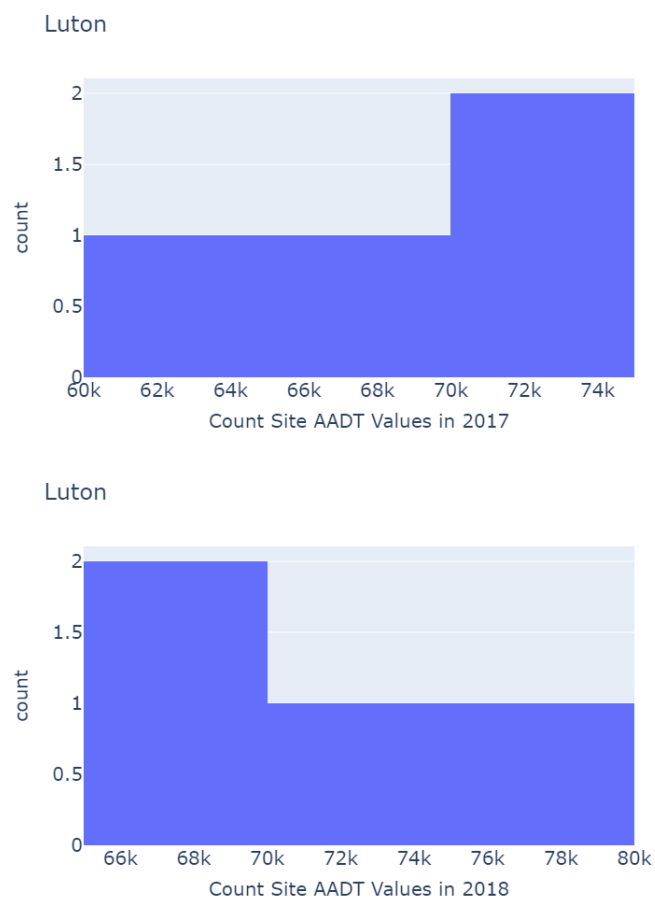
Table A.1: Satellite Imagery Datasets Summary Table

## Appendix B

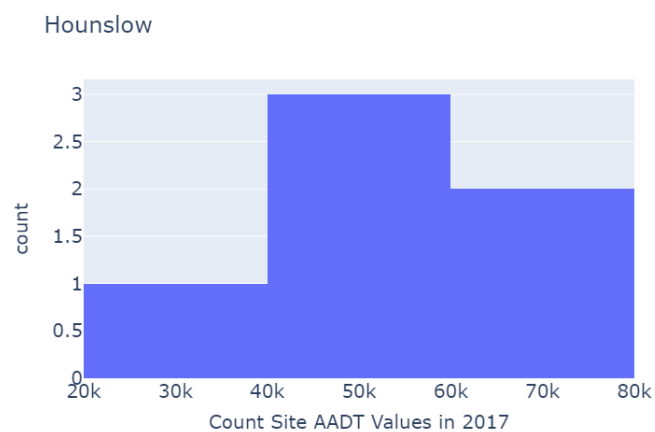
### Chosen LA's Maximum Count Site AADT Values 2017 and 2018 Years



**Figure B.1:** Trafford AADT Count Site Histograms



**Figure B.2:** Luton AADT Count Site Histograms



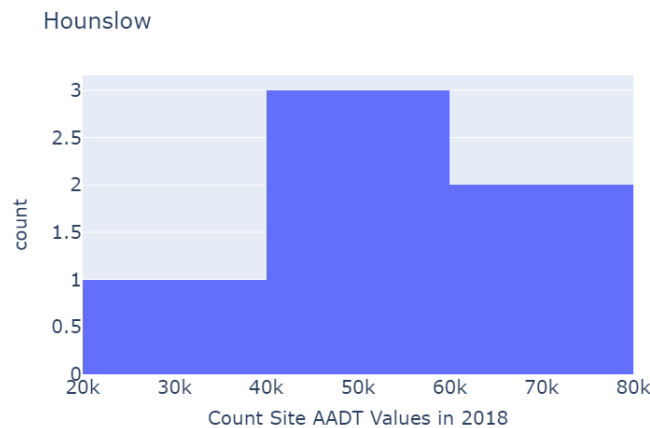


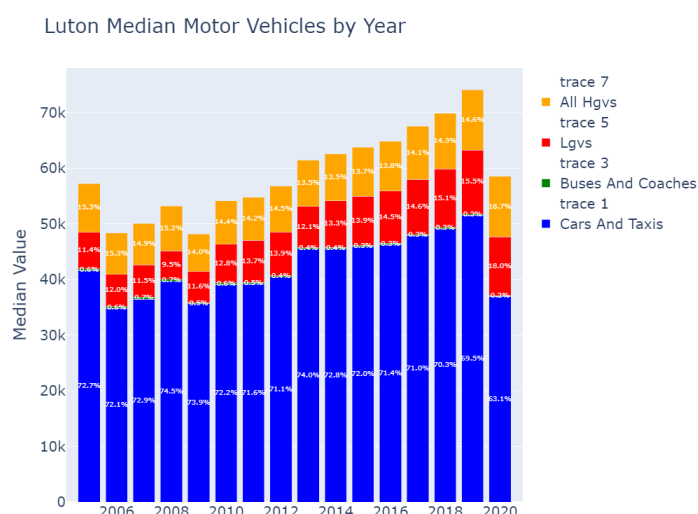
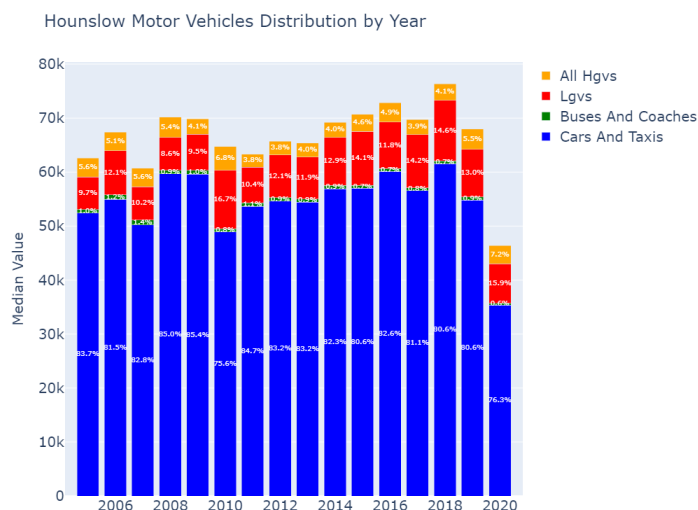
**Figure B.3:** Hounslow AADT Count Site Histograms



**Figure B.4:** Blackburn AADT Count Site Histograms

## Appendix C

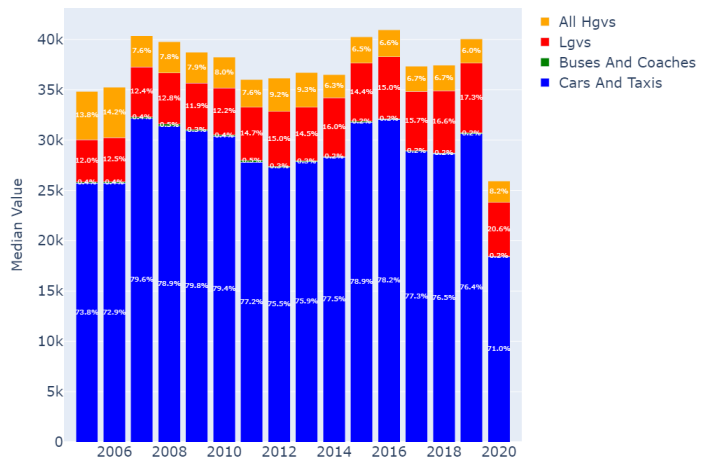
### Chosen LA's AADT Vehicle Type Distributions



## Chapter C. Chosen LA's AADT Vehicle Type Distributions

---

Blackburn with Darwen Motor Vehicles Distribution by Year



Trafford Motor Vehicles Distribution by Year

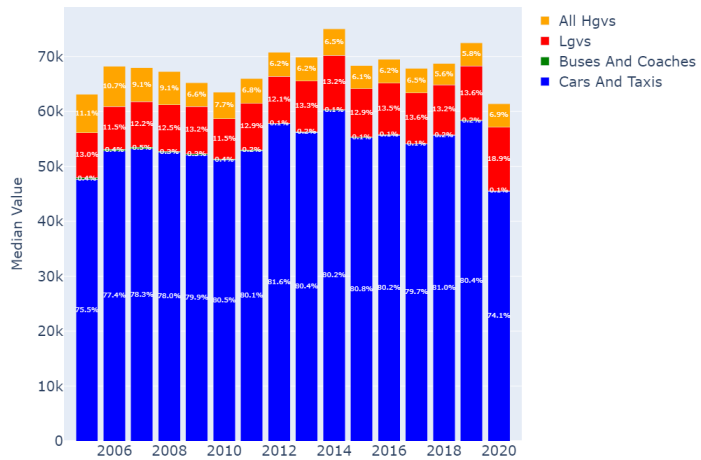


**Figure C.1:** Chosen LA's AADT by Vehicle Type Distributions

# Appendix D

## A-Roads LA AADT and GHG Emissions Per Year

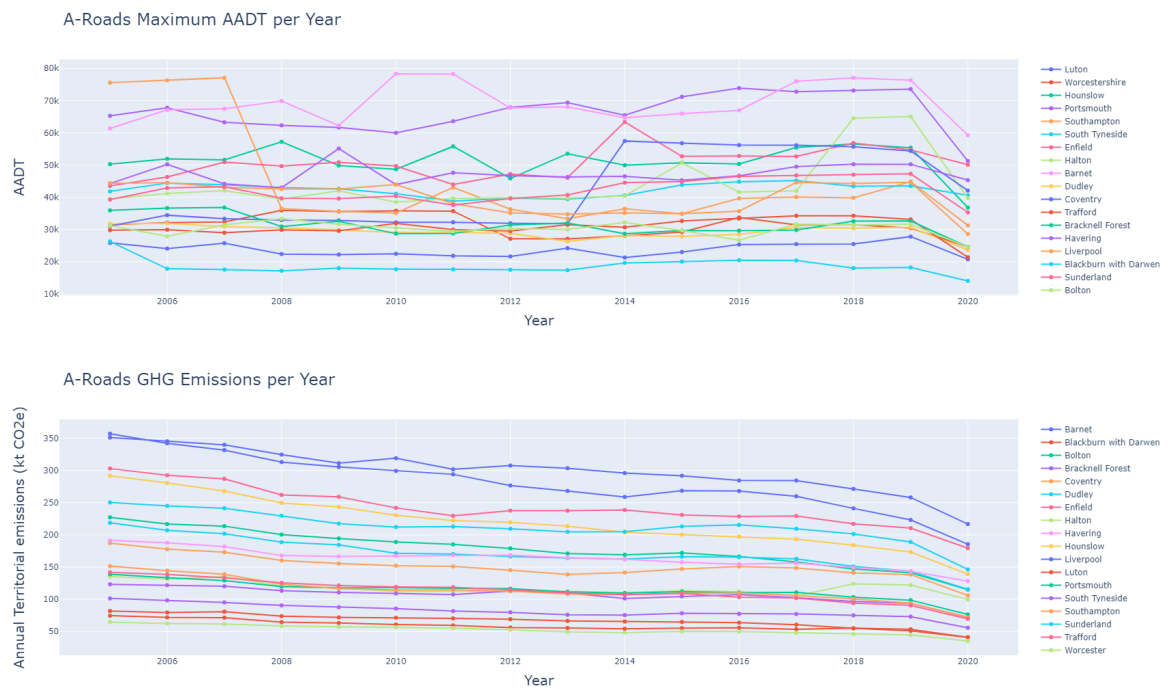


**Figure D.1: LA A-Roads AADT and GHG per year**

## Appendix E

# Minor Roads LA AADT and GHG Emissions Per Year



**Figure E.1:** LA Minor Roads AADT and GHG Emissions per year

## Appendix F

# Havering A-Roads and Minor Roads Vehicle Distributions

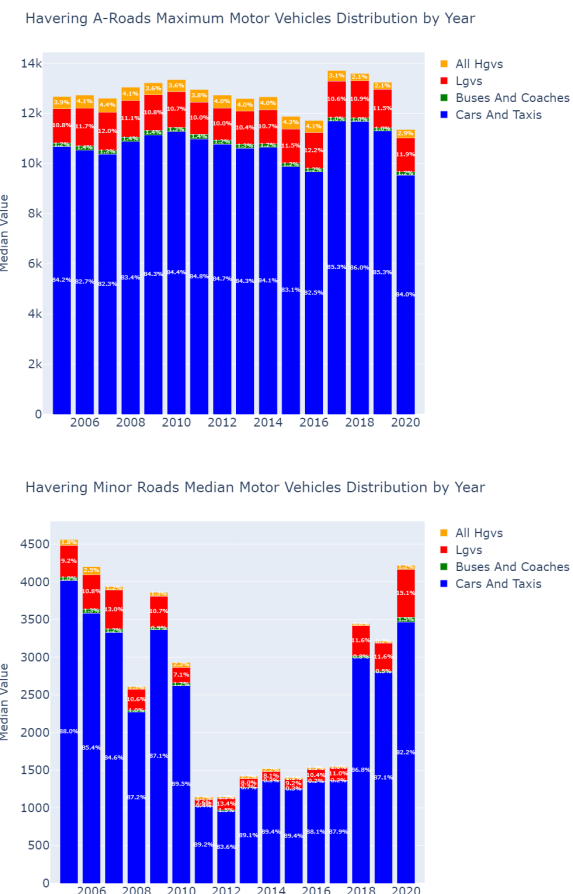


**Figure F.1:** Havering A-Roads and Minor Roads Vehicle Type Distributions

## Appendix G

### Chosen LA WV-2 Satellite Images Before Processing



**Figure G.1:** Trafford LA WV-2 Satellite Image Before Processing



**Figure G.2:** Luton LA WV-2 Satellite Image Before Processing



**Figure G.3:** Hounslow LA WV-2 Satellite Image Before Processing



**Figure G.4:** Blackburn LA WV-2 Satellite Image Before Processing

## Appendix H

### Chosen LA WV-2 Satellite Images After Processing

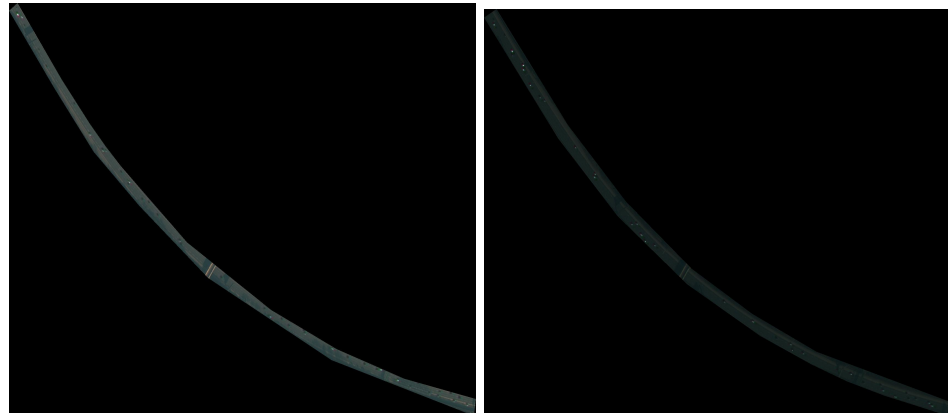
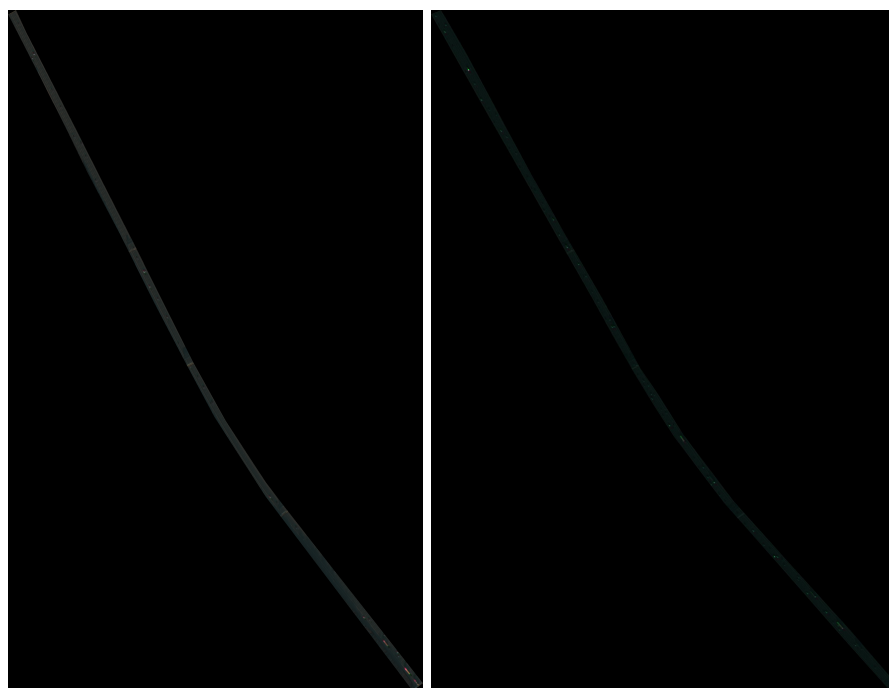
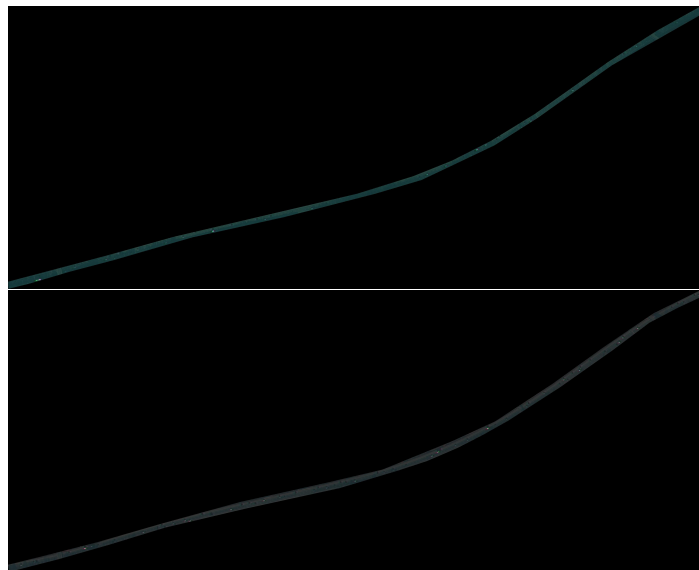


Figure H.1: Trafford LA WV-2 Satellite Images After Processing



**Figure H.2:** Luton LA WV-2 Satellite Images After Processing



**Figure H.3:** Hounslow LA WV-2 Satellite Images After Processing

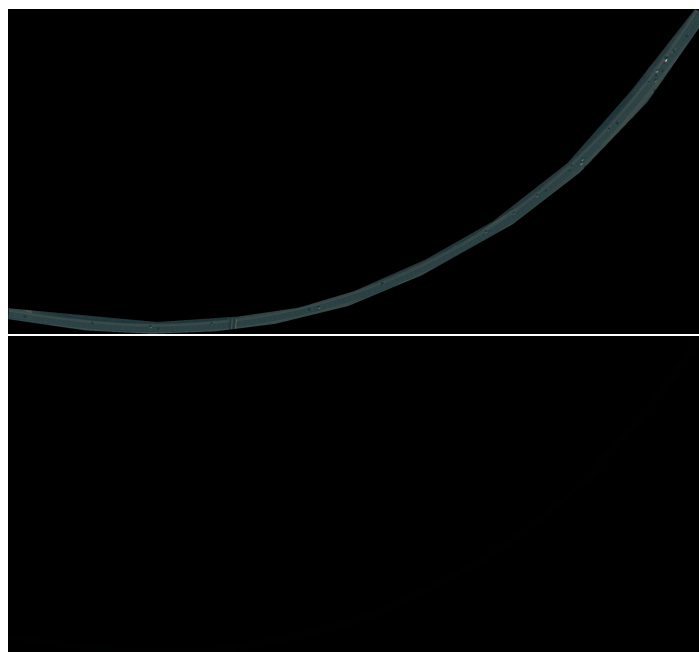


**Figure H.4:** Blackburn LA WV-2 Satellite Images After Processing

# Appendix I

## YOLOv5 Road Vehicle xView Training Results

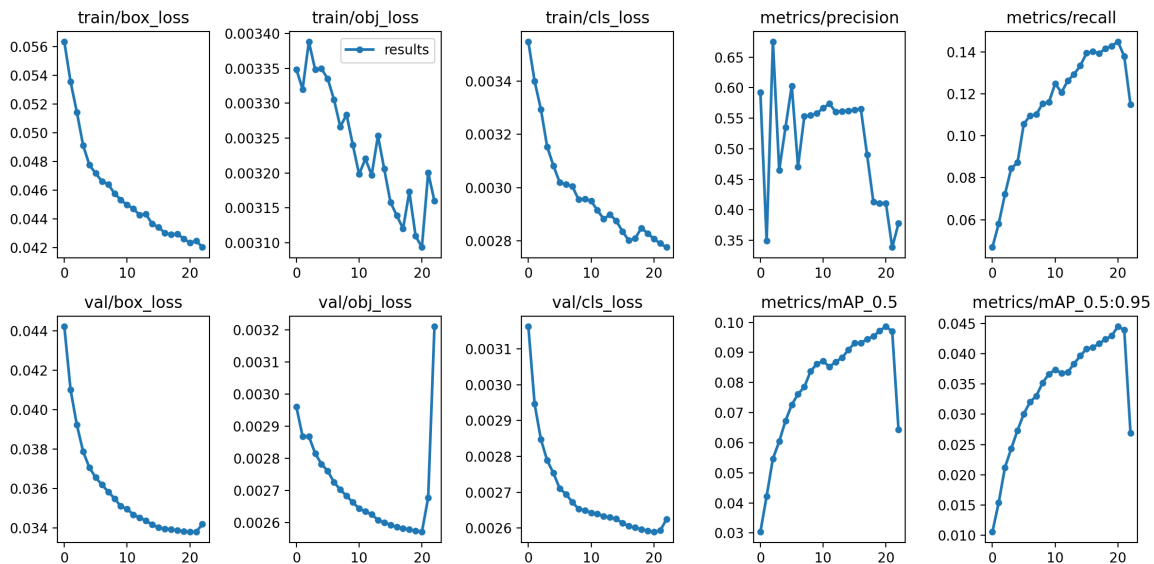


**Figure I.1:** YOLOv5 Training Results

# Appendix J

## ANN AADT Model Architecture

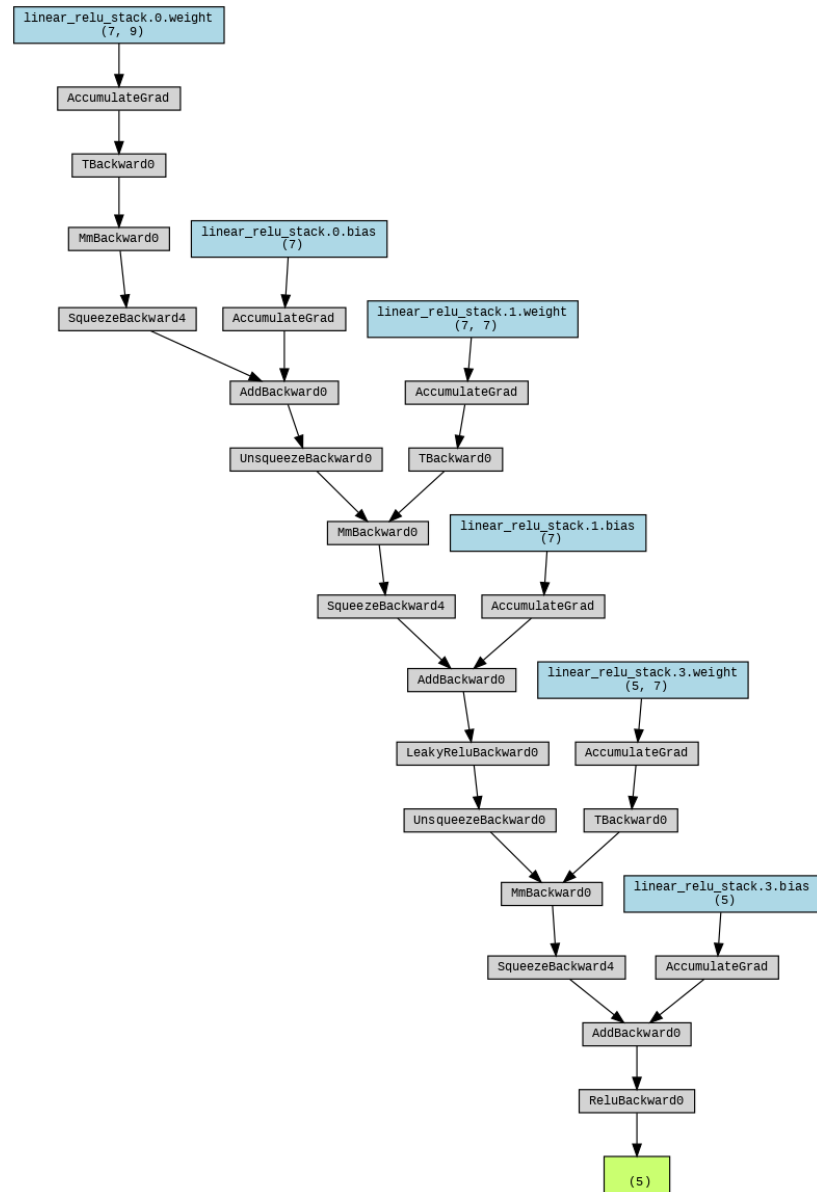


Figure J.1: ANN AADT Model Architecture

# Appendix K

## LA AADT Training and Validation Curves



Figure K.1: Trafford M60/9083A LA Train and Val Curves

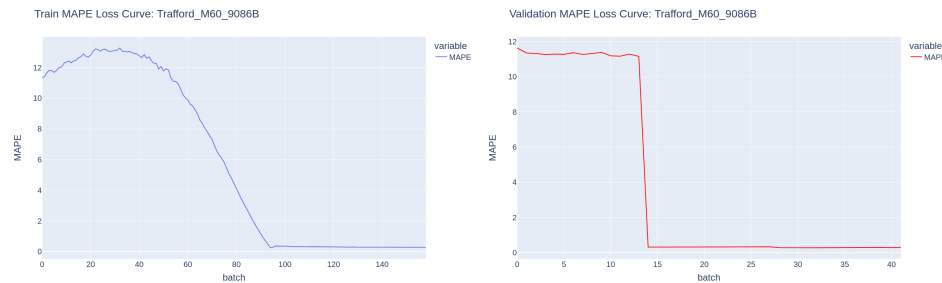


Figure K.2: Trafford M60/9083B LA Train and Val Curves

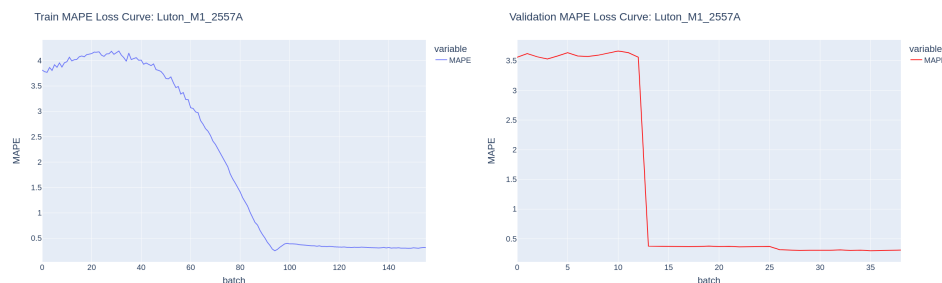
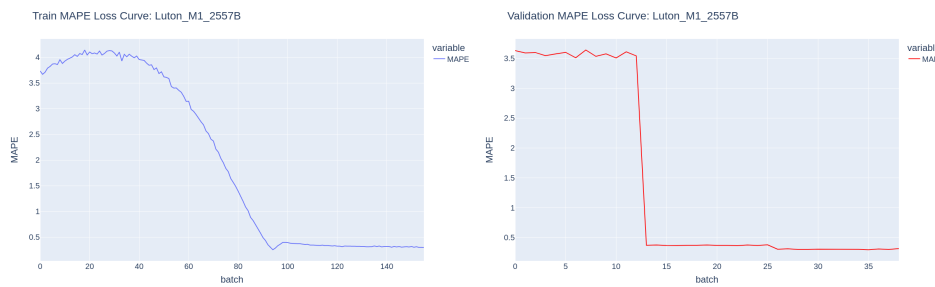
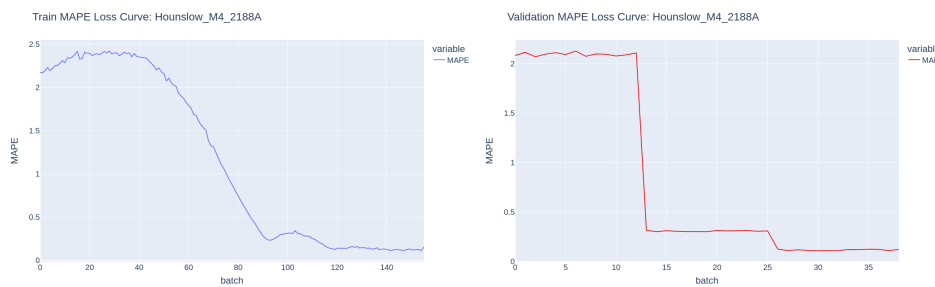


Figure K.3: Luton M1/2557A LA Train and Val Curves



**Figure K.4:** Luton M1/2557B LA Train and Val Curves



**Figure K.5:** Hounslow M4/2188A LA Train and Val Curves

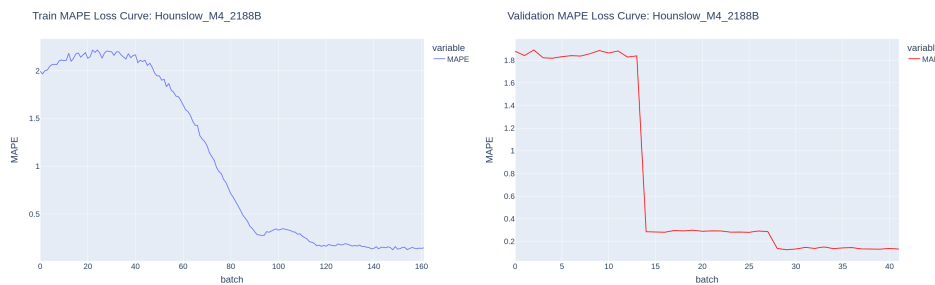


**Figure K.6:** Hounslow M4/2188B LA Train and Val Curves

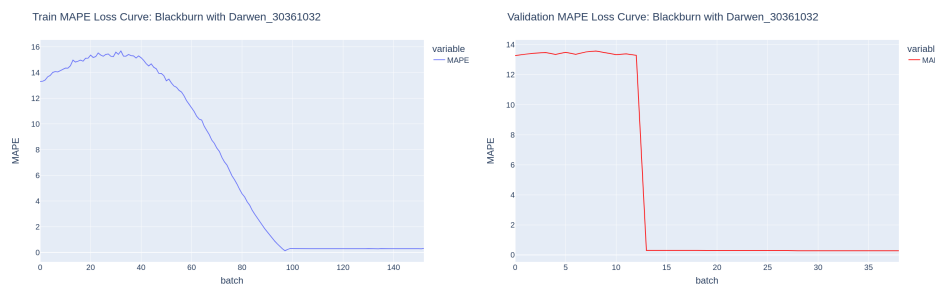


**Figure K.7:** Blackburn 30361032 LA Train and Val Curves



**Figure K.8:** Blackburn 30361033 LA Train and Val Curves

## Appendix L

### Motorways No Vehicle Type Scatter Plot

Motorways No Vehicle Type AADT vs GHG Emissions for Chosen LAs

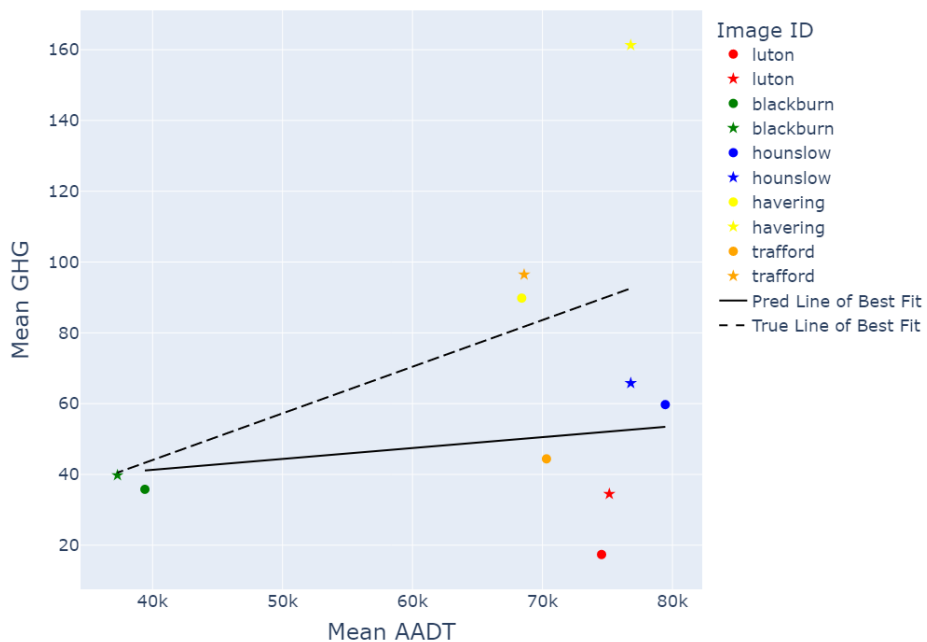
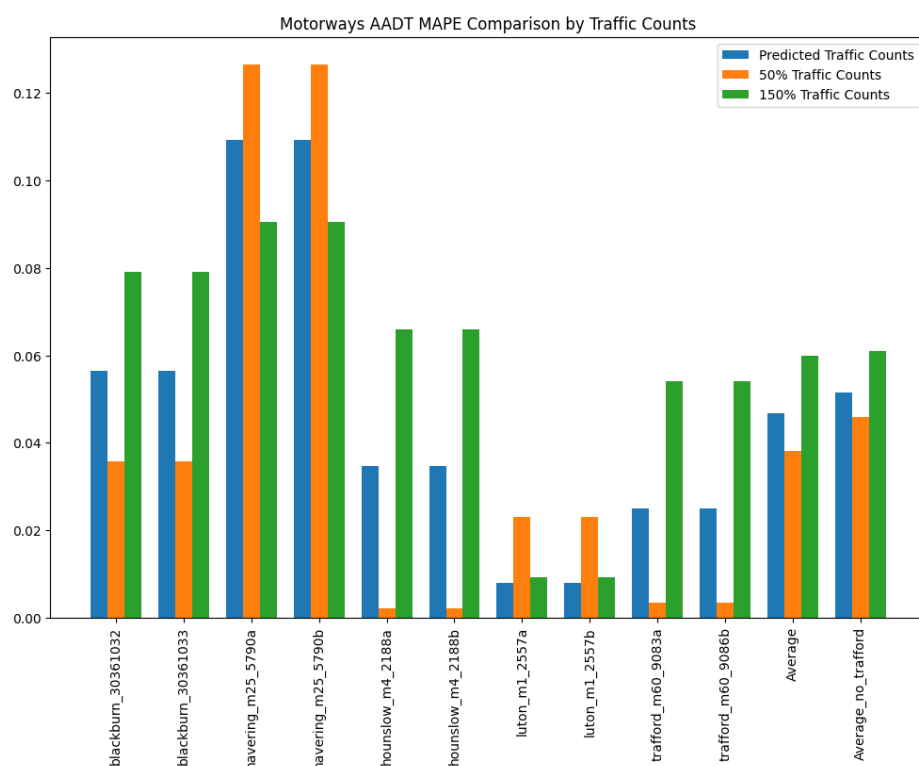


Figure L.1: Motorways No Vehicle Type Scatter Plot

## Appendix M

# Traffic Counts and Speed AADT Parametric Analysis



**Figure M.1:** Effect of Traffic Counts on AADT MAPE

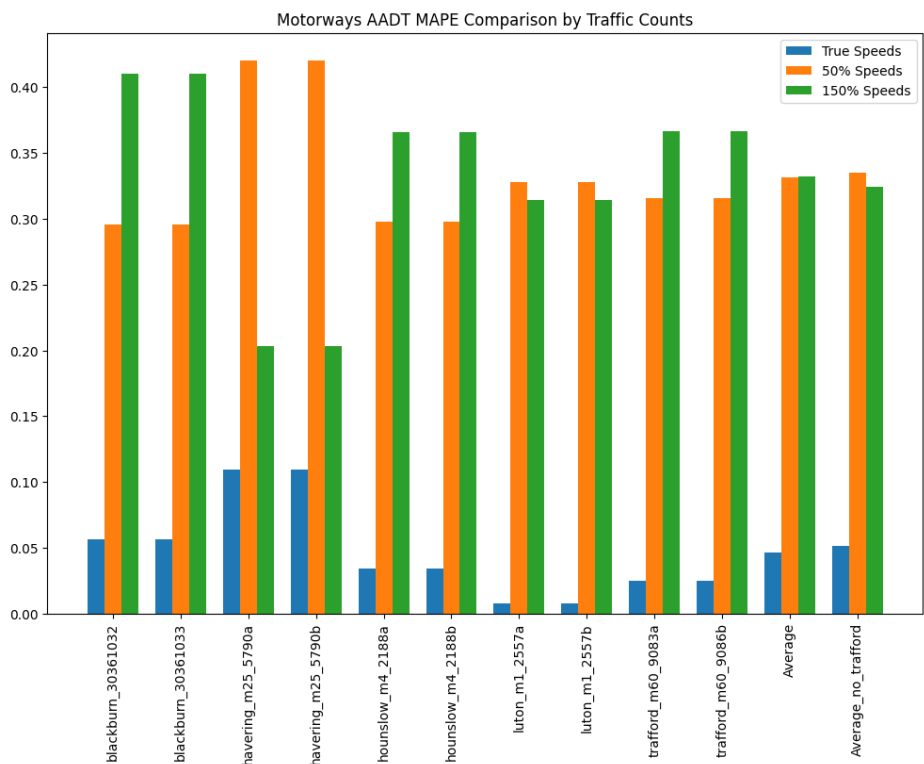


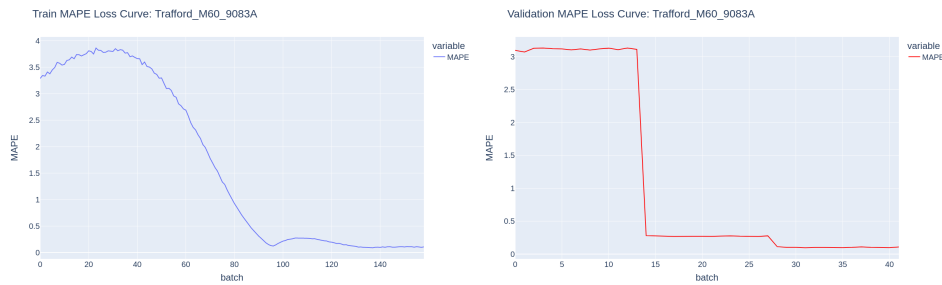
**Figure M.2:** Effect of Speed on AADT MAPE

# Appendix N

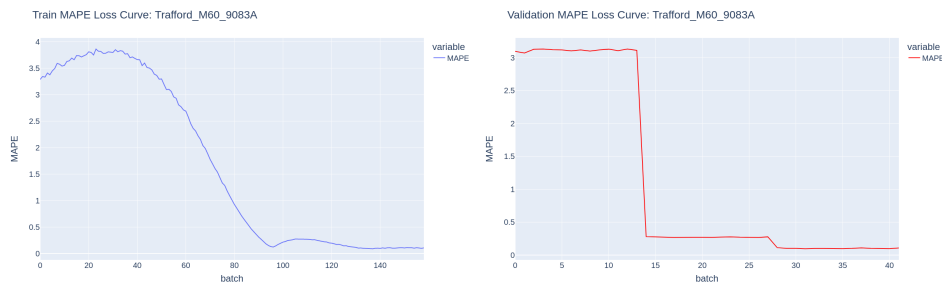
## A-Roads ANN AADT Training and Validation Curves



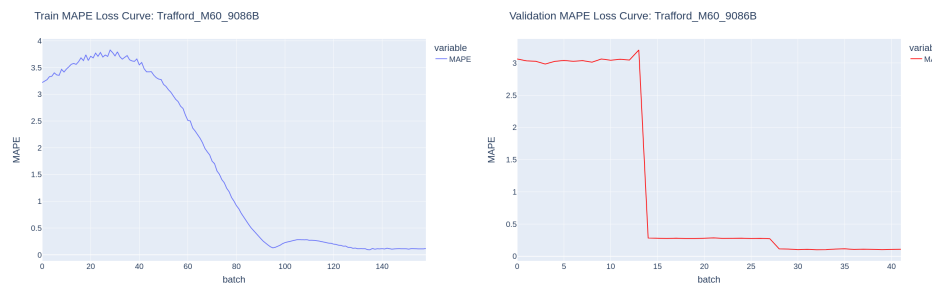
**Figure N.1:** Havering M25/590A LA A-Roads Train and Val Curves



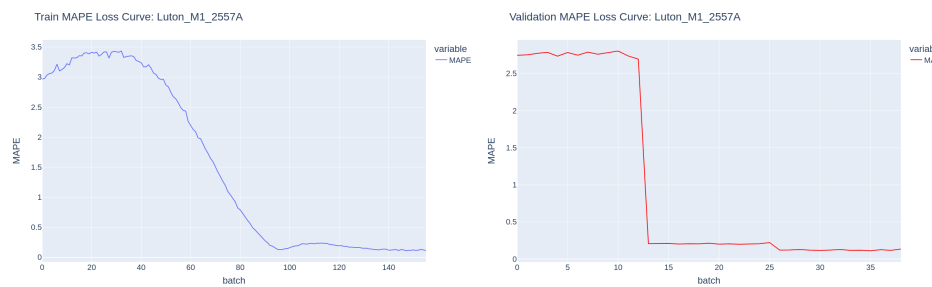
**Figure N.2:** Havering M25/590A LA A-Roads Train and Val Curves



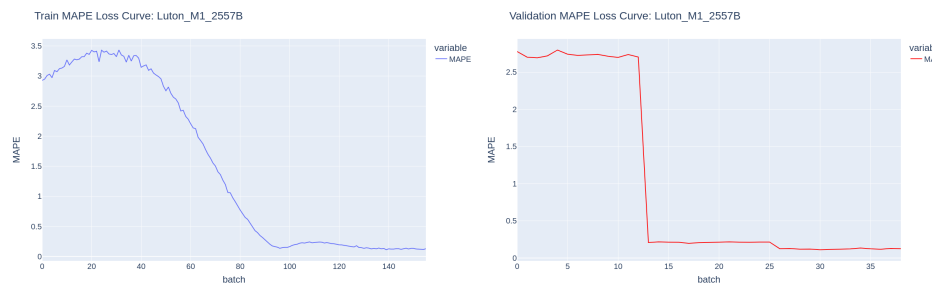
**Figure N.3:** Trafford M60/9083A LA A-Roads Train and Val Curves



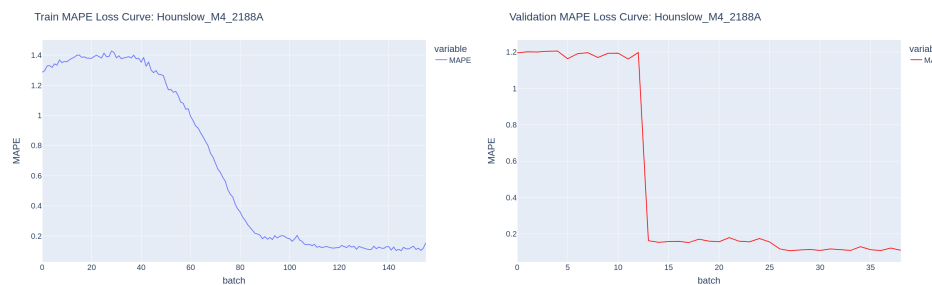
**Figure N.4:** Trafford M60/9083B LA A-Roads Train and Val Curves



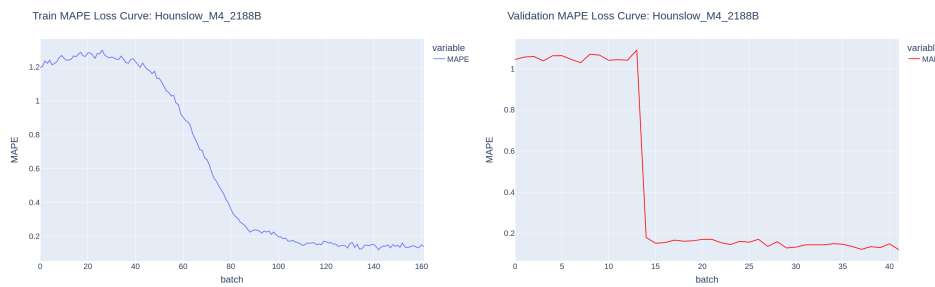
**Figure N.5:** Luton M1/2557A LA A-Roads Train and Val Curves



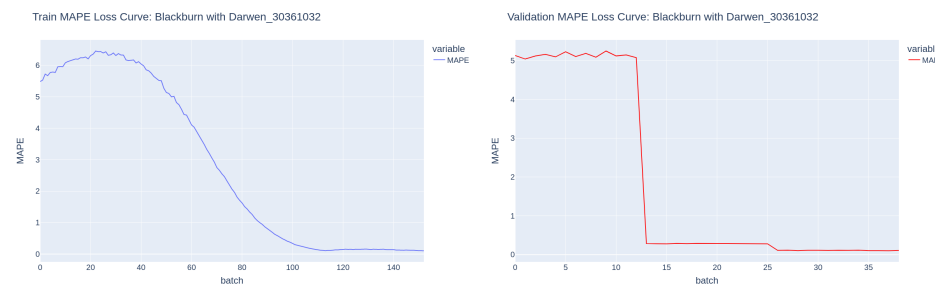
**Figure N.6:** Luton M1/2557B LA A-Roads Train and Val Curves



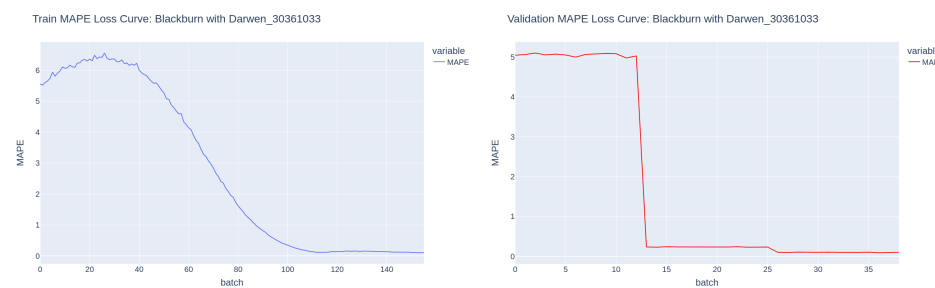
**Figure N.7:** Hounslow M4/2188A LA A-Roads Train and Val Curves



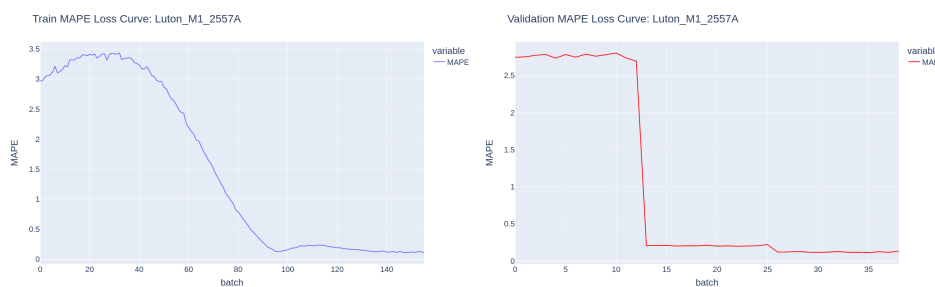
**Figure N.8:** Hounslow M4/2188B LA A-Roads Train and Val Curves



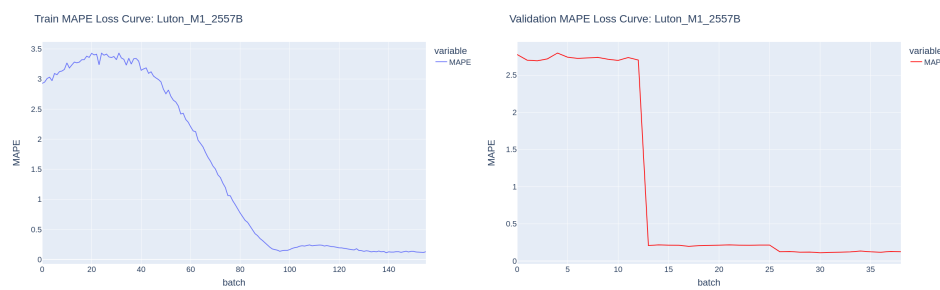
**Figure N.9:** Blackburn 30361032 LA A-Roads Train and Val Curves



**Figure N.10:** Blackburn 30361033 LA A-Roads Train and Val Curves



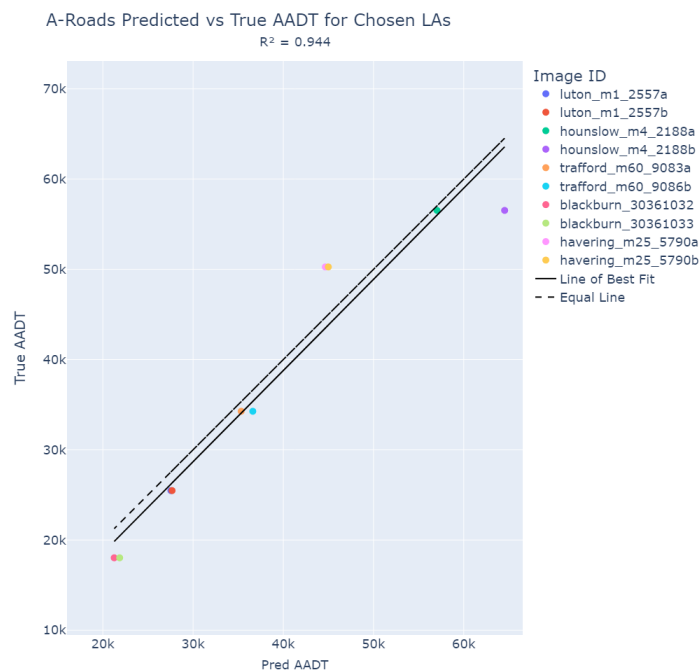
**Figure N.11:** Luton M1/2557A LA A-Roads AADT Training and Validation Curves



**Figure N.12:** Luton M1/2557B LA A-Roads AADT Training and Validation Curves

## Appendix O

# A-Roads LA AADT and GHG Emissions Results



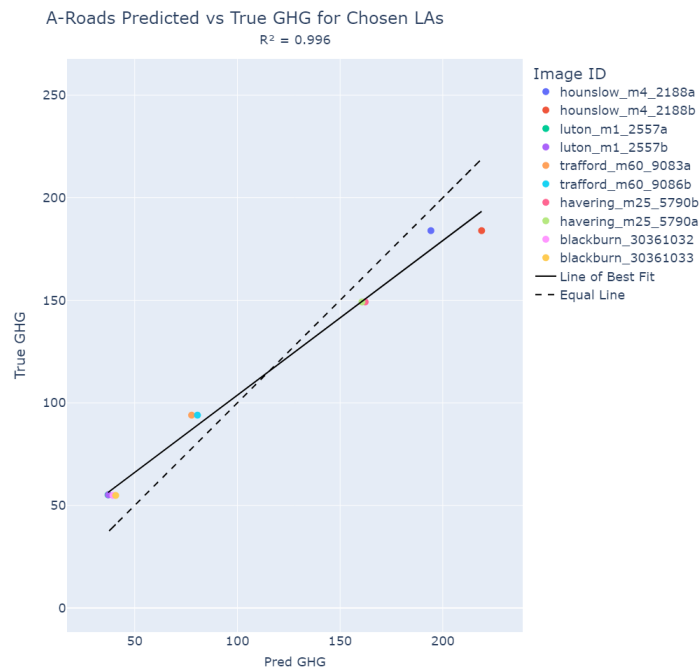


**Figure O.1:** LA A-Roads Predicted vs True AADT (top) and GHG Emissions (bottom) Scatter Plots

## Appendix P

# Minor Roads LA AADT and GHG Emissions Results

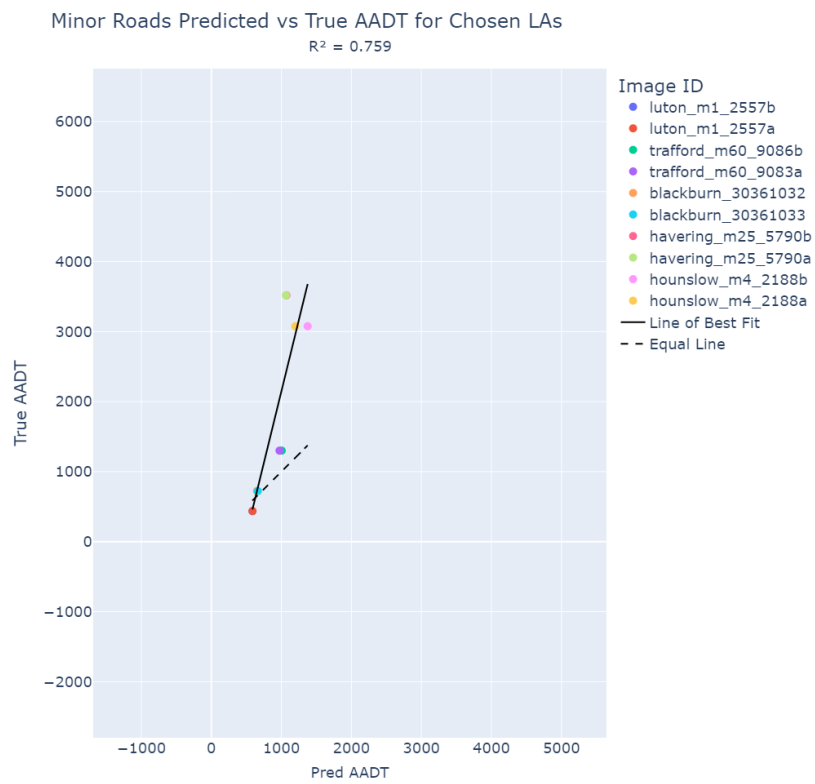


**Figure P.1:** Minor Roads AADT Scatter Plot Results

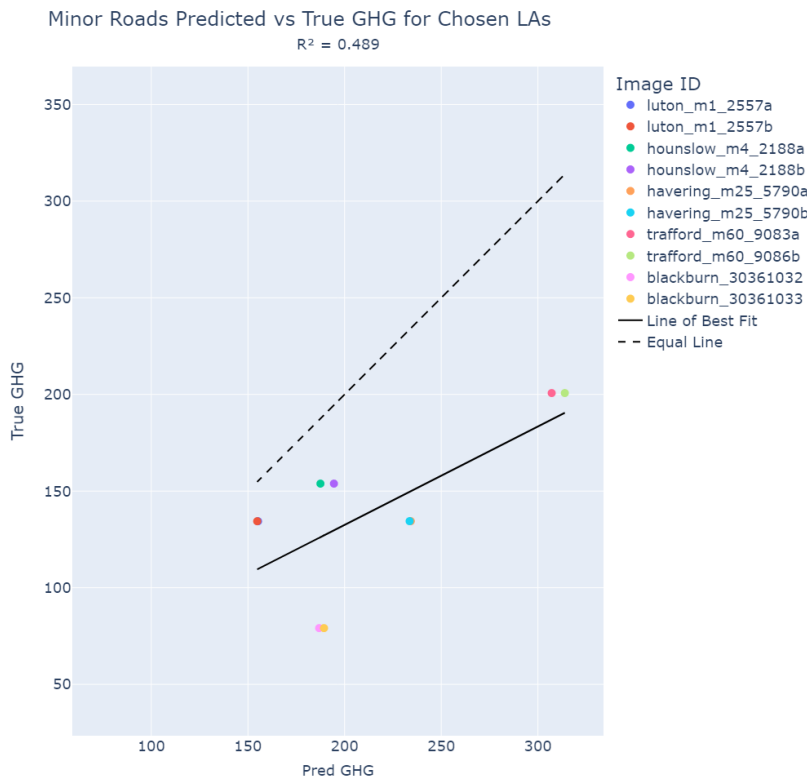


**Figure P.2:** Minor Roads GHG Emissions Scatter Plot Results

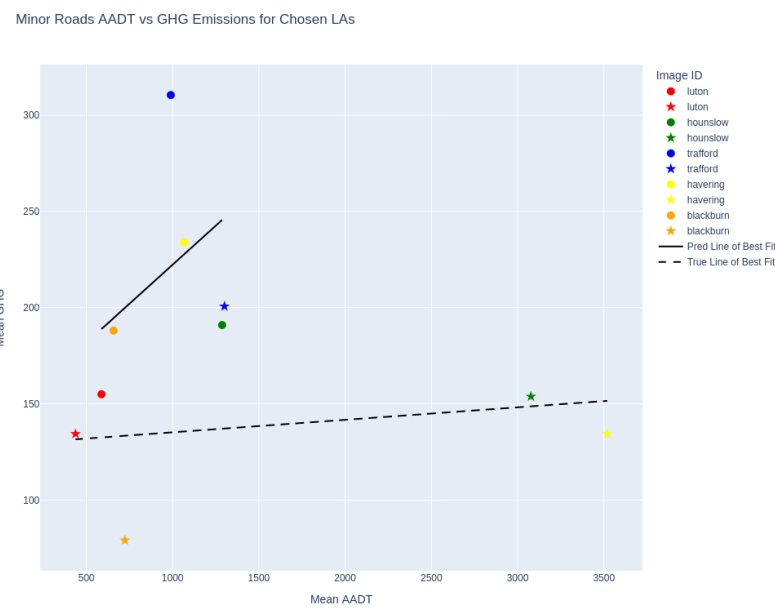


**Figure P.3:** Minor Roads AADT vs GHG Results